Accepted Manuscript

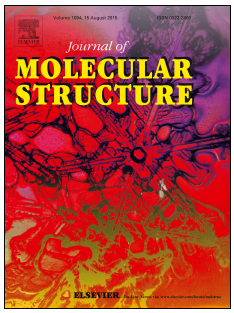

A novel porphyrin derivative and its metal complexes: Electrochemical, photoluminescence, thermal, DNA-binding and superoxide dismutase activity studies

Savaş Purtaş, Muhammet Köse, Ferhan Tümer, Mehmet Tümer, Ayşegül Gölcü, Gökhan Ceyhan

PII: S0022-2860(15)30313-6

DOI: 10.1016/j.molstruc.2015.10.013

Reference: MOLSTR 21858

To appear in: *Journal of Molecular Structure*

Received Date: 19 August 2015

Revised Date: 8 October 2015

Accepted Date: 19 October 2015

Please cite this article as: S. Purtaş, M. Köse, F. Tümer, M. Tümer, A. Gölcü, G. Ceyhan, A novel porphyrin derivative and its metal complexes: Electrochemical, photoluminescence, thermal, DNA-binding and superoxide dismutase activity studies, *Journal of Molecular Structure* (2015), doi: 10.1016/j.molstruc.2015.10.013.

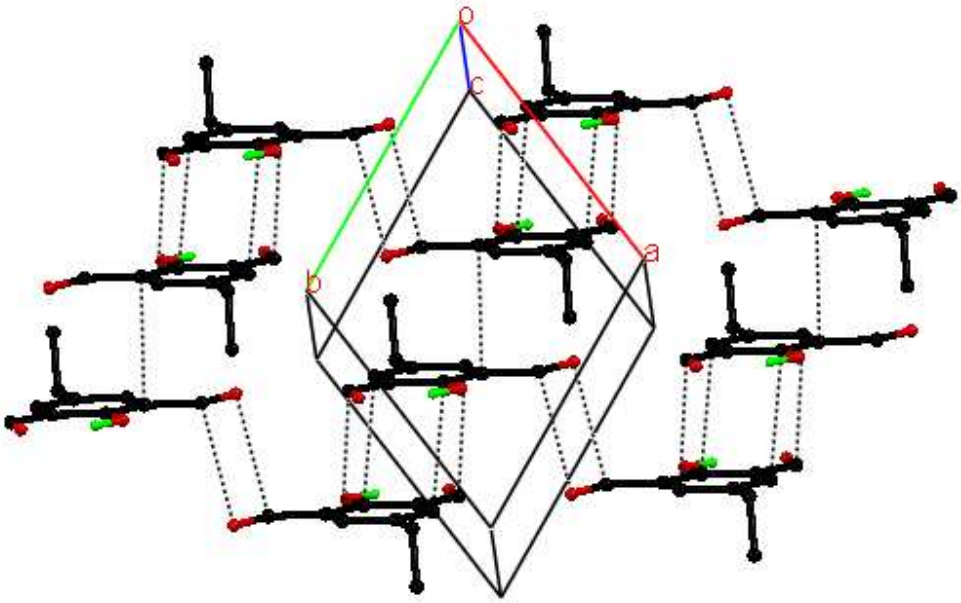

In this study, in order to synthesize the novel porphyrin Schiff base ligand, we prepared both 4-ethyl-2,6-bis(hydroxymethyl)phenol and 4-ethyl-2,6-diformylphenol compounds. The porphyrin Schiff base ligand is a novel compound. The compounds (A) and (B) were characterized by the analytical and spectroscopic methods. Single crystals of these compounds were obtained from the $CHCl_3$-EtOH solution by the slow evaporation and their structural characterizations were, first time, done by X-ray crystallography technique.

A novel porphyrin derivative and its metal complexes: Electrochemical, photoluminescence, thermal, DNA-binding and superoxide dismutase activity studies

Savaş Purtaş, Muhammet Köse, Ferhan Tümer, Mehmet Tümer, Ayşegül Gölcü, Gökhan Ceyhan

Chemistry Department, K.Maras Sütcü Imam University, 46100, K.Maras, Turkey

Abstract

In this study, a new porphyrin-Schiff base ligand (L) and its metal complexes (Cu(II), Fe(III), Mn(III), Pt(II) and Zn(II)) were synthesized. The starting material 4-ethyl-2,6-bis(hydroxymethyl)phenol (A) was synthesized from 4-ethylphenol and formaldehyde in the alkaline media. The compound (A) was then oxidized to the 4-ethyl-2,6-diformylphenol (B). The starting compounds (A) and (B) were obtained as single crystals. Structures of the compounds (A) and (B) were determined by the X-ray crytallography technique. The porphyrin ligand (L) and its metal complexes were characterized by the analytical and spectroscopic methods. Electronic, electrochemical and thermal properties of the synthesised compounds were investigated. Superoxide dismutase activities (SOD) of the porphyrin Schiff base complexes were investigated and results were discussed. Additionally,the DNA (fish sperm FSdsDNA) binding studies of the complexes were performed using UV-vis spectroscopy. Competitive studies with ethidium bromide (EB) show that the compounds interact efficiently with DNA through an intercalating way.

Keywords: Porphyrin-Schiff base, X-ray, superoxide dismutase activity, DNA-binding

Corresponding author: Mehmet Tümer
Tel.: +90 344 280 14 44, **Fax:** +90 344 280 13 52,
E-mail address: mtumer@ksu.edu.tr

1. Introduction

Porphyrin compounds are the heterocyclic organic molecules and composed of four modified pyrrole subunits inter-connected at their α-carbon atoms *via* methine bridges (=CH−). Porphyrins are probably the most significant and common class of natural pigments [1-3]. With their considerable chromophore structure and molecular symmetry metal porphyrins have a noteable interest in their own right to physicists and chemists [4]. Tetraphenyl porphyrins have assumed a privilege role in various areas of disciplines, ranging from molecular semiconductors [5] to non-linear optics [6]: in particular several features, such as chemical and thermal stability, make porphyrins selectable as encouraging materials for gas sensing applications. Unsymmetrical porphyrin, particularly tetraphenyl porphyrin derivatives substituted having an expanded π-conjugated system at the *meso*-position, are very interesting compopunds. There are some reports about porphyrin-Schiff base ligands and their metal complexes [7,8].

DNA intercalators are generally small planar molecules including coherent aromatic rings [9]. Nevertheless, the porphyrins are also known to bind and intercalate within DNA [10]. The porphyrin ring system is larger and more complex than that of other known intercalators and poses some fascinating questions for DNA-ligand interactions [11-14]. Mn(III), Fe(III) and Zr(III) complexes bind only by a non-intercalative mechanism to AT-rich regions of DNA, however the metal-free ligand and its Cu(II) and Ni(II) complexes bind intercalatively to GC-rich sequences and with less choice at TA sequences.

Copper and zinc containing Cu/ZnSOD enzyme is the maximum influential catalytic diversity found in the mammalian cell plasma and extracellular spaces. This SOD enzym catalyzes the dismutation of superoxide radical (O_2^-) into molecular oxygen and hydrogen peroxide *via* one electron redox cycle. With respect to normal cells, cancer cells have been considered to cause large amount of $O_2^{\bullet -}$ production in the cell [15] and the SOD activity in cancer cell was found to be lower than the normal cell [16-17]. Thus, synthetic SOD mimics can be taken account of as an excellent device in mediating apoptosis by mentioning oxidative stress caused by $OH^{\bullet}$ radical.

In this work, a novel porphyrin-Schiff base ligand 4-ethyl-2,6-bis[5-(4-iminophenyl)-10,15,20-triphenylporphyrin]phenol (L) and its Cu(II), Fe(III), Mn(III), Pt(II) and Zn(II) complexes were synthesized (Scheme) and characterized by the elemental analyses, MALDI-TOF mass, $^1H(^{13}C)$NMR spectra, FT-IR and UV-vis spectra. Single crystals of both 4-ethyl-2,6-bis(hydroxymethyl)phenol and 4-ethyl-2,6-diformylphenol compounds were obtained. Their molecular structures were, first time, characterized by single crystal X-ray diffraction

technique. Electrochemical, photoluminescence and thermal properties of the porphyrin Schiff base ligand (L) and its metal complexes were investigated. SOD activities and DNA binding properties of the porphyrin Schiff base ligand and its metal complexes were investigated.

2. Experimental

2.1. Materials and measurements

All reagents and solvents were of reagent-grade quality and obtained from commercial suppliers (Aldrich or Merck). Elemental analyses (C,H,N) were performed using a LECO CHNS 932. Infrared spectra were obtained using KBr disc (4000-400 cm^{-1}) on a Perkin Elmer Spectrum 100 FT-IR. The electronic spectra in the 200–900 nm range were obtained on a Perkin Elmer Lambda 45 spectrophotometer. ^{1}H and ^{13}C NMR spectra were recorded on a Bruker 400 MHz instrument and TMS was used as an internal standard and $CDCl_3$ as solvent. The thermal studies of the compounds were performed on a Perkin Elmer STA 6000 simultaneous Thermal Analyzer under nitrogen atmosphere at a heating rate of 10 °C/min. The mass spectra of complexes were obtained in dihydroxybenzoic acid as MALDI Matrix using nitrogen laser accumulating 50 laser shots using Bruker Microflex LT MALDI TOF mass spectrometer.

The single-photon fluorescence spectra of the porphyrin-Schiff base compound (H_2L) and its metal complexes were collected on a Perkin Elmer LS55 luminescence spectrometer. All samples were prepared in spectrophotometric grade solvents and analysed in a 1 cm optical path quartz cuvette.

Cyclic voltammograms were recorded on a Iviumstat Electrochemical workstation equipped with a low current module (BAS PA–1) recorder. The electrochemical cell was equipped with a BAS glassy carbon working electrode (area 4.6 mm^2), a platinum coil auxiliary electrode and a Ag^+/AgCl reference electrode filled with tetrabutylammonium tetrafloroborate (0.1 M) in DMF and CH_3CN solution and adjusted to 0.00 V vs SCE. Cyclic voltammetric measurements were performed at room temperature in an undivided cell (BAS model C–3 cell stand) with a platinum counter electrode and an Ag^+/AgCl reference electrode (BAS). All potentials are reported with respect to Ag^+/AgCl. The solutions were deoxygenated by passing dry nitrogen through the solution for 30 min prior to the experiments, and during the experiments the flow was maintained over the solution. Digital simulations were performed using DigiSim 3.0 for windows (BAS, Inc.). Experimental cyclic voltammograms used for the fitting process had the background subtracted and were corrected electronically for ohmic drop. Mettler Toledo MP 220 pH meters was used for the pH

measurements using a combined electrode (glass electrode reference electrode) with an accuracy of ±0.05 pH.

Data collection for X-ray crystallography was completed using a Bruker APEX2 CCD diffractometer and data reduction was performed using Bruker SAINT [18]. SHELXS97 and SHELXL2014/6 were used to solve and refine structures, respectively [19].

2.2. Preparation of the 4-ethyl-2,6-bis(hydroxymethyl)phenol (A)

4-Ethylphenol (25.0 g, 0.17 mol) was added to a stirred warm (70 °C) solution of NaOH (10.60 g, 0.27 mol) in THF (200 mL). To the stirring mixture *p*-formaldehyde (45.0 g, 0.61 mol) was added and the mixture was stirred for 48 h at room temperature. THF was removed on a rotary evaporator. The resulting solid was dissolved in distilled water (100 mL), acidified with HCI (0.5 M) and extracted with diethylether. The diethylether solution was dried over Na_2SO_4 and the solvent was removed on a rotary evaporator. The white crystalline product was collected and dried in vacuo. (29.50 g, 67%). ^{1}HNMR ($CDCl_3$, TMS): δ 6.90 (s, 2H, Ar-H), 4.80 (s, 4H, -CH_2OH), 2.60-2.55 (q, 2H, -CH_2-), 1.19-1.23 (t, 3H, CH_3). ^{13}CNMR ($CDCl_3$, TMS): δ 125.94-152.60 (Ar-C), 63.70 (-CH_2O), 27.94 (-CH_2), 15.80 (-CH_3). FTIR(KBr)/cm^{-1}: 3407 (CH_2OH), 3325 (Ph-OH), 2973 (aryl CH), 1635, 1506 (aryl C-C).

2.2. Preparation of the 4-ethyl-2,6-diformylphenol (B)

Activated MnO_2 (40 g) was added to $CHCl_3$ (200 mL) in a 500 mL round bottom flask equipped with an overhead stirrer and a water-cooled condenser. The mixture was heated to reflux with stirring about 15 min, then the powder of the 4-ethyl-2,6-bis(hydroxymethyl)phenol (5 g) was added. After being kept refluxing for 24 h, the reaction was cooled to room temperature and filtered. The solid was washed by $CHCl_3$ (40 mL x 5) thoroughly until the filtrate was colorless. Then the filtrate was concentrated on a rotary evaporator yielding a yellow solid. (2.62 g, 53%)

^{1}HNMR ($CDCl_3$, TMS): δ 9.10 (s, 2H, carbonyl-H), 7.70 (s, 2H, Ar-H), 2.57-2.58 (q, 2H, -CH_2-), 1.20-1.23 (t, 3H, CH_3). ^{13}CNMR ($CDCl_3$, TMS): δ 190.45 (carbonyl-C), 125.30-151.55 (Ar-C), 27.92 (-CH_2), 15.83 (-CH_3). FTIR(KBr)/cm^{-1}: 3345 (Ph-OH), 2965 (aryl CH), 1660 (C=O), 1603, 1596 (aryl C-C).

2.3. Preparation of the 5,10,15,20-tetraphenylporphyrin (TPP)

TPP was synthesized by the known methods [20]. Melting point: > 200 °C. δ_H ($CDCl_3$)/ppm: 8.85 (s, 8H, pyr-CH), 8.29 (m, 8H, 4 x C_6H_5), 7.77 (m, 12H, 4 x C_6H_5), -2.71

(s, 2H, pyrrole internal NH). FTIR (KBr, ν, cm^{-1}): 3311 (NH), 3021 (aryl C-H), 1594 $(CH=N)_{porphyrin}$, 1553 ($C-C)_{aryl}$, 1347 (C=C). UV-Vis [Toluene, λ_{max}(nm), ε_{max} ($M^{-1}cm^{-1}$)]: 416 nm (4.30 x 10^5), 515 (1.30 x 10^4), 550 (4.23 x 10^4), 592 (1.71 x 10^4), 648 (0.55 x 10^4).

2.4. Preparation of the 5-(4-Nitrophenyl)-10,15,20-triphenylporphyrin (TPP-NO_2)

TPP-NO_2 was obtained by the reaction of TPP and sodium nitrite in trifluoroacetic acid according to the known method [21]. Melting: point > 200 °C. ^{1}H-NMR: δ_H ($CDCl_3$)/ppm: 8.87 (m, 6H, pyr-CH), 8.77 (d, 2H, pyr-CH), 8.69 (m, 2H, C_6H_4), 8.40 (m, 2H, C_6H_4), 8.24 (m, 6H, 3 x C_6H_5), 7.75 (m, 9H, 3 x C_6H_5), -2.72 (s, 2H, pyrrole internal NH). FTIR (KBr, ν, cm^{-1}): 3315 (NH), 2988 (C-H), 1594 $(CH=N)_{porphyrin}$, 1557 $(C-C)_{aryl}$, 1515, 1344 (NO_2), 1344 (C=C). UV-Vis [Toluene, λ_{max}(nm), ε_{max} ($M^{-1}cm^{-1}$)]: 418 (4.10 x 10^5), 514 (3.11 x 10^4), 549 (0.95 x 10^4), 589 (0.88 x 10^4), 646 (0.75 x 10^4).

2.5. Synthesis of 5-(4-aminophenyl)-10,15,20-triphenylporphyrin (TPP-NH_2)

TPP-NH_2 was obtained by the reduction of TPP-NO_2 using $SnCl_2.2H_2O$ as a reducing agent in concentrated hydrochloric acid [22]. ^{1}HNMR ($CDCl_3$) δ: 8.93 (d, 2H, β-pyrrole), 8.86 (d, 2H, β-pyrrole), 8.85 (s, 4H, β-pyrrole), 8.20 (m, 6H, *o*-triphenyl), 8.01 (d, 2H, 4-aminophenyl), 7.76 (m, 9H, *m*-/*p*-triphenyl), 7.09 (d, 2H, 4-aminophenyl), 4.04 (s, 2H, amino), -2.72 (s, 2H, pyrrole internal NH). FTIR (KBr, ν, cm^{-1}): 3318 (NH), 2973 (C-H), 1615 $(CH=N)_{pyrrole}$, 1506 $(C-C)_{aryl}$, 1349 (C=C).

2.6. Preparation of 4-ethyl-2,6-bis[5-(4-iminophenyl)-10,15,20-triphenylporphyrin]phenol (L)

The porphyrin Schiff base ligand was synthesized as follows: TPP-NH_2 (0.2 mmol, 126 mg) and the 4-ethyl-2,6-diformylphenol aldehyde compound (0.1 mmol, 178 mg) was dissolved in 100 ml of dry toluene containing 4 Å molecular sieves. The resulting solution was refluxed until the disappearance of the TPP-NH_2, monitored by TLC (30 h). The solvent was removed under reduced pressure and the crude product was dissolved in CH_2Cl_2 and filtered. Evaporation of the solvent gave purple solid. The obtained product was purified from $CHCl_3$-hexane (v/v, 1/3) solvent mixture. $C_{98}H_{68}N_{10}O$, yield: 68%, Melting: point > 200 °C. Color: purple. Elemental analyses: Found (calcd.)%: C, 84.02 (83.98), H, 4.85 (4.89), 10.95 (9.99). ^{1}HNMR ($CDCl_3$) δ (ppm): 8.93 (d, 2H, β-pyrrole), 8.88 (s, 4H, β-pyrrole), 8.71 (d, 2H, β-pyrrole), 8.68 (s, H, CH=N (imine)), 8.45 (m, 6H, *o*-triphenyl-H), 8.02-7.80 (m, 9H+2H, (*m*-phenyl-H) + (*p*-phenyl-H) + aminophenyl), 7.65 (s, 2H, diformyl-H), 2.61-2.59 (q, 2H, -CH_2-part of ethyl group), 1.25-1.22 (t, 3H, CH_3-part of ethyl group), -2.70 (s, 2H, pyrrole

internal NH). ^{13}C-NMR ($CDCl_3$) δ (ppm): 15.80, 27.88, 107.55, 110.30, 117.14, 119.65, 121.92, 126.85, 128.06, 134.54, 135.10, 141.65, 146.25, 150.26, 154.27, 164.90. FTIR (KBr, ν, cm^{-1}): 3324 (NH), 2973 $(CH)_{aliphatic}$, 1617 (CH=N), 1575 $(C\text{-}C)_{aryl}$, 1492 $(CH{=}N)_{pyrrole}$, 1349 (C=C). MALDI-TOF-MS, (m/z): Calculated: 1401.65; Found: 1402 $[C_{98}H_{68}N_{10}O]^+$.

2.7. Preparation of the Cu(II), Fe(III), Mn(III), Pt(II) and Zn(II) *metal complexes of the 4-ethyl-2,6-bis[5-(4-iminophenyl)-10,15,20-triphenylporphyrin]phenol (L)*

The porphyrin Schiff base ligand (0.5 mmol, 0.700 g) was dissolved in CH_2Cl_2 (20 mL) solution and followed by addition metal salts [2 mmol, 0.273 g for $ZnCl_2$; 0.342 for $CuCl_2.2H_2O$; 0.542 for $FeCl_3.6H_2O$; 0.830 g for $K_2[Pt(Cl)_4]$; 0.464 g for $Mn(AcO)_3$] in CH_3OH (20 mL). The reaction solution was refluxed for about 1 h. The extent of the reaction was monitored by measuring the UV–Vis spectrum of the reaction solution every 10 min. After cooling to room temperature, 200 mL distilled water was added to the reaction mixture and extracted three times. Purity of the complexes were checked by t.l.c. studies.

LCu_4Cl_3: Yield: 87.6%, green solid. M.p. > 300 °C. Anal. Calcd. For $[C_{98}H_{63}N_{10}OCl_3Cu_4]$: C, 66.99; H, 3.61; N, 7.97 %; found: C, 67.06; H, 3.67; N, 7.92 %. FTIR (KBr, ν, cm^{-1}): 3021 $(C\text{-}H)_{aromatic}$, 2922, 2840 $(C–H)_{aliphatic}$, 1619 $(CH{=}N)_{imine}$, 1530 $(C\text{-}C)_{aromatic}$, 1281 $(C–O)_{phenolic}$, 1002 $(Cu\text{-}N)_{porphyrin}$,565 (M-O), 462 (M-N). MALDI-TOF-MS, (m/z): Calculated: 1757.15; Found: 1757.15 $[C_{98}H_{63}N_{10}OCl_3Cu_4]^+$.

LPt_4Cl_3: Yield: 83.2 %, purple red solid. M.p. > 300 °C; Anal. Calcd. For $[C_{98}H_{63}N_{10}OCl_3Pt_4]$: C, 51.55; H, 2.78; N, 6.13 %; found: C, 51.60; H, 2.84; N, 6.17. FTIR (KBr, ν, cm^{-1}): 3015 $(C\text{-}H)_{aromatic}$, 2918, 2850 $(C–H)_{aliphatic}$, 1610 $(CH{=}N)_{imine}$, 1518 $(C\text{-}C)_{aromatic}$, 1250 $(C–O)_{phenolic}$, 1007 $(Pt\text{-}N)_{porphyrin}$, 558 (M-O), 450 (M-N). MALDI-TOF-MS, (m/z): Calculated: 2283.31; Found: 2284.57 $[C_{98}H_{63}N_{10}OCl_3Pt_4]^+$.

LZn_4Cl_3: Yield: 65.4%, purple red solid. M.p. > 300 °C. Anal. Calcd. For $[C_{98}H_{63}N_{10}OCl_3Zn_4]$: C, 66.70; H, 3.60; N, 7.94 %; found: C, 66.75; H, 3.55; N, 7.88 %. FTIR (KBr, ν, cm^{-1}): 3021 $(C\text{-}H)_{aromatic}$, 2935, 2844 $(C–H)_{aliphatic}$, 1621 $(CH{=}N)_{imine}$, 1520 $(C\text{-}C)_{aromatic}$, 1227 $(C–O)_{phenolic}$, 1005 $(Zn\text{-}N)_{porphyrin}$, 580 (M-O), 456 (M-N). MALDI-TOF-MS, (m/z): Calculated: 1764.61; Found: 1765.08 $[C_{98}H_{63}N_{10}OCl_3Zn_4]^+$.

$LFe_3Cl_4(H_2O)$: Yield: 81.3%, purple red solid. M.p. > 300 °C. Anal. Calcd. For $[C_{98}H_{65}N_{10}O_2Cl_4Fe_3]$: C, 68.28; H, 3.80; N, 8.12 %; found: C, 68.34; H, 3.86; N, 8.17 %. FTIR (KBr, ν, cm^{-1}): 3023 $(C\text{-}H)_{aromatic}$, 2930, 2845 $(C–H)_{aliphatic}$, 1615 $(CH{=}N)_{imine}$, 1544 (C-

C)$_{aromatic}$, 1230 (C–O)$_{phenolic}$, 1002 (Fe-N)$_{porphyrin}$, 530 (M-O), 450 (M-N). MALDI-TOF-MS, (m/z): Calculated: 1723.97; Found: 1724.54 $[C_{98}H_{65}N_{10}O_2Cl_4Fe_3]^+$.

$LMn_3(AcO)_4(H_2O)$: Yield: 80.1%, purple black solid. M.p. > 300 °C. Anal. Calcd. for $[C_{106}H_{77}N_{10}O_{10}Mn_3]$: C, 70.12; H, 4.27; N, 7.71 %; Found: C, 70.18, H, 4.32; N, 7.77 %. FTIR (KBr, ν, cm^{-1}): 3024 (C-H)$_{aromatic}$, 2925, 2850 (C–H)$_{aliphatic}$, 1680 (C=O)$_{acetic\ acid}$, 1610 (CH=N)$_{imine}$, 1547 (C-C)$_{aromatic}$, 1240 (C–O)$_{phenolic}$, 1011 (Mn-N)$_{porphyrin}$, 570 (M-O), 460 (M-N). MALDI-TOF-MS, (m/z): Calculated: 1815.62; Found: 1625.5 $[C_{106}H_{77}N_{10}O_{10}Mn_3\text{-}Mn(AcO)_2(H_2O)]^+$.

2.8. X-ray Structural Determination

The structural properties of the starting compounds (A) and (B) were determined by X-ray diffraction technique. Data for the starting compounds (A) and (B) were collected at 150(2)K° on a Bruker ApexII CCD diffractometer using Mo-Kα radiation (λ= 0.71073Å). The structures were solved by direct methods and refined on F^2 using all the reflections [19]. All the non-hydrogen atoms were refined using anisotropic atomic displacement parameters and hydrogen atoms bonded to the carbon atoms were inserted at calculated positions using a riding model. Hydrogen atom bonded to oxygen atoms were located from difference maps and allowed to refine with temperature factors. Details of the crystal data and refinement are given in Table 1. All the bond lengths and angles are within the normal ranges. All bond lengths and angles in the phenyl ring have normal C*sp2*- C*sp2* values with small distortions. Bond lengths and angles for the starting compounds (A) and (B) are given in the supplementary file.

2.9. Superoxide dismutase (SOD) activity studies of the transition metal complexes

SOD assay kit-WST was used to evaluate SOD activities of the complexes. In this method, xanthine oxidase aerobically oxidases xanthine to urate, producing $O_2^{\cdot-}$ in the process. 2-(4-Iodophenyl)-5-(2,4-disulfophenyl)-2*H*-tetrazolium, monosodium salt (WST-1) scavenges the $O_2^{\cdot-}$ formed in the reaction, which causes the reduction of the colourless WST-1 to the yellow WST-1 formazan. WST-1 formazan has a characteristic absorbance peak at 440 nm, therefore, quantitative reduction of WST-1 to WST-1 formazan by $O_2^{\cdot-}$ was monitored spectrophotometrically at pH 7.8 on a UV-160A UV–Vis. Spectrophotometer, Shimadzu (Japan) at 440 nm and 25 ºC for 20 min. In the presence of the complex being tested, the absorbance values (at 440 nm) of the WST-1 formazan decrease. This is due to the complex competes with the WST-1 to scavenge the $O_2^{\cdot-}$. The rate of absorption changes was

determined and the percent inhibition (IC_{50}) of WST reduction to WST-1 formazan was calculated. The WST-1 assay is an indirect method of analysis because the extent of the reduction of the appearance of the yellow WST-1 formazan in the presence of a SOD mimic is taken as a measure of SOD activity [23]. All reagents were obtained from Sigma–Aldrich Chemical Co. Ltd. and assays were run in 1 mL of solution.

2.10. DNA binding studies of the ligand and its metal complexes

Double-strand FSdsDNA (Sigma) was used as received. The stock solution of DNA was prepared by dissolving appropriate amount of DNA in Tris-HCl buffer (20 mM Tris–HCl, 20 mM NaCl, pH 7.0) by gentle stirring at room temperature and stored at 4 ºC for no longer than a week. The ratio of the UV absorbance at 260 and 280 nm (A_{260}/A_{280}) was checked to be ca. 1.86, indicating that the DNA is sufficiently free from protein contamination. The DNA concentration per nucleotide phosphate [NP] was determined by the UV absorbance [24] at 260 nm after 1:20 dilutions using the known ε value of 6600 $M^{-1}cm^{-1}$.

3. Results and Discussion

3.1 Characterization of starting materials

In this study, in order to obtain a novel porphyrin Schiff base ligand (L), the 4-ethyl-2,6-bis(hydroxymethyl)phenol (A) and 4-ethyl-2,6-diformylphenol (B) compounds were synthesized and characterized by the analytical and spectroscopic methods. Single crystals of these compounds were obtained from the $CHCl_3$-EtOH solution by slow evaporation and their structural characterizations were, first time, determined by X-ray crystallography technique. Analytical and spectroscopic data of the compounds (A) and (B) are given in the experimental section. In the ^1H NMR spectrum of the starting compound (A), the signal at the 6.90 ppm may be assigned to the two protons of the aromatic ring. The methylene protons of the $-CH_2O$ groups are shown at the 4.80 ppm. The CH_3 and CH_2 protons of the ethyl group on the aromatic ring were shown as multiplets in the 1.19-1.23 and 2.55-2.60 ppm range, respectively. In the ^{13}C NMR spectrum, the signals in the 125.94-152.60 ppm range can be attributed to the aromatic ring carbon atoms. The signals at the 63.70, 27.94 and 15.80 ppm may be assigned to the carbon atoms of the CH_2O, $-CH_2$ and $-CH_3$ groups, respectively. In the FTIR spectrum of the (A), the OH vibrations of the aliphatic CH_2OH and phenolic Ph-OH groups were shown at the 3407 and 3325 cm^{-1}, respectively. In the ^1H NMR spectrum of the

dicarbonyl compound (B), the signal at 9.10 ppm may be assigned to the protons of the carbonyl groups. The aromatic ring protons were shown at the 7.70 ppm. The CH_3 and CH_2 protons were shown as multiplets in the 1.20-1.23 and 2.57-2.58 ppm range, respectively. In the ^{13}C NMR spectrum, the carbon atoms of the carbonyl groups were shown at the 190.45 ppm. The signals in the 125.30-151.55 ppm range can be attributed to the aromatic carbon atoms. The aliphatic carbon atoms were shown at the 27.92 ($-CH_2$) and 15.83 ppm ($-CH_3$). In the FTIR spectrum of the compound (B), the vibration band at the 3345 cm^{-1} can be attributed to the phenolic OH group. The vibration of the carbonyl group were shown at the 1660 cm^{-1}.

3.2 X-ray structures of 4-ethyl-2,6-bis(hydroxymethyl)phenol(A) and 4-ethyl-2,6-diformylphenol (B)

The structure of the (A) was solved in *monoclinic* crystal system, *P2(1)/c* space group with R_{final} value of 0.0408. Molecular structure of the compound (B) is shown in Fig. 1. The asymmetric unit contains two independent molecules differing in the conformation of alcohol arms and hydrogen bonding interactions within the structure. The C–O bond distances in the structure are in well agreement with similar structures with different substitute groups on the *p*- position [25-27]. The molecules form centrosymmetric dimers held together by two complementary hydrogen bonds (Fig. 2). The structure is stabilised by intermolecular O–H$\cdots$O hydrogen bonds resulting in a 2D hydrogen bond network and the compound does not show intra-molecular hydrogen bonding within the structure. There are also π-π stacking interactions between the two adjacent aromatic rings with a centroid–centroid separation of 4.100 A°. Packing diagram of the starting compound (B) are shown in Fig. 2.

Perspective view of the compound (A) is shown in Fig. 3. The compound (A) crystallizes in *triclinic* crystal system, $P\,\bar{1}$ space group with unit cell parameters a= 7.6563(6), b= 7.8598(7), c= 8.4085(7) Å, α= 73.2310(10), β= 71.0790(10), γ= 66.6050(10)°, V=431.81(6) $Å^3$ and Z=2. The aldehyde (C1=O1 and C10=O3) distances are 1.211(14) and 1.2253(14) Å respectively, which are in the range of C=O double bond character and in good agreement with literature values of similar compounds [28,29]. The phenolic group (Ph-OH) involves in intra-molecular hydrogen bonding with one of the aldehyde groups (O2$\cdots$O3= 2.6508(12) Å) forming a S(6) hydrogen bonding motif. Two aldehyde molecules are linked by two inter-molecular complementary hydrogen bonds O2–H2$\cdots$O3 [-x+1,–y,–z+2] resulting in a $D_2^2(4)$ hydrogen bonding motif (Fig. 3). Weaker hydrogen bond type CH$\cdots$O interactions were also observed in the structure. Hydrogen bonded dimers are linked by π-π

interactions within the structure. Crystal packing of the compound is determined by π-π interactions (Fig. 4).

3.3 Characterization of the porphyrin-Schiff base ligand (L) and its complexes

5-(4-Aminophenyl)-10,15,20-triphenylporphyrin (TPP-NH_2) was prepepared by the reduction of nitro analogue 5-(4-nitrophenyl)-10,15,20-triphenylporphyrin (TPP-NO_2). TPP-NH_2 was then used to prepare the porphyrin Schiff base ligand 4-ethyl-2,6-bis[5-(4-iminophenyl)-10,15,20-triphenylporphyrin]phenol (L). Although the TPP-NH_2 compound has the assymmetric nature, synthesized porphyrin Schiff base ligand (L) has the symmetric structure. Purification of the porphyrin based compounds is considerably hard and therefore, the yields of these compounds are very low. Crystallization technique is not suitable in the purification of TPP, TPP-NO_2 and TPP-NH_2 because these compounds are soluble in same solvents. Therefore, the column chromatography method was used for this purpose. The ligand (L) is soluble in THF, DMF, DMSO, toluene, CH_2Cl_2, *etc*. The ligand and its metal complexes are very stable compounds at room temperature without decomposing. There are a few reports about porphyrin Schiff base ligand and its metal complexes obtained from the 5-(4-aminophenyl)-10,15,20-tris(4-nitrophenyl)porphyrin and 4-formylphenol derivative [30]. These compounds are called as “Push-Pull Porphyrins”.

All porphyrine derivatives were characterized by the analytical and spectroscopic methods. Proposed structures of the porphyrin Schiff base ligand and its complexes were given in Scheme. In order to determine the structure of the porphyrin Schiff base ligand (L), $^1H(^{13}C)$ NMR spectra have been carried out and obtained data are given in the experimental section. ^1H NMR spectrum of the ligand was measured in deuterated chloroform ($CDCl_3$) as a solvent. In the spectrum of the porphyrin Schiff base ligand, the eight protons of β-pyrrole separated into two groups, which exhibited the two β-pyrrolic protons near C=N groups were in a different chemical environment to the another six protons. The signals at 8.93, 8.88 and 8.71 ppm can be attributed to the β-pyrrole protons. This signal is located at a very low field as the delocalization of electron on the pyrrole ring. The unsymmetrical chemical environment of these protons exhibited the influence of the extended π structure or the strong electron donating effect of the ethoxy and hydroxy groups. A singlet at 8.68 ppm may be assigned to the proton of the CH=N group of the porphyrin Schiff base ligand (L). The protons of the phenyl rings bonded on the porphyrin ring were shown as multiplet in the 8.45-7.80 ppm range. The protons of the diformyl ring were shown as a singlet signal at 7.65 ppm. The signals in the 2.61-2.59 ppm range can be attributed to the protons of the –CH_2- group.

The triplets in the 1.25-1.22 ppm range may be assigned to -CH_3 protons. The singlet of the NH peak (due to rapid exchange of N-H protons) is found to be very high field (-2.70 ppm), since they are located within the shielded core of the porphyrin ring.

^{13}C NMR spectrum of the ligand (L) shows six sharp signals (121.92 (C_{meso}), 126.85 ($C_{m,m'}$), 128.06 (C_p), 134.54 (C_β), 135.10 ($C_{o,o'}$), 141.65 ($C_{p'}$) ppm) and a very broad signal (146.25 ppm) for α-carbon atoms. The carbon atom of the azomethine group was shown at 164.90 ppm. The signals at 15.80 and 27.88 ppm can be attributed to the carbon atoms of the ethyl group on the diformyl ring.

In order to investigate the mass spectral properties of the ligand and its metal complexes, MALDI-TOF-MS studies were performed. The MALDI-TOF spectrum of the ligand (L) is shown in Fig. 5 and obtained data are given in the experimental section. The spectra of the Cu(II) and Mn(III) complexes are given in the supplemantary material. As seen from the obtained data, the MALDI-MS spectra results confirm the proposed structures for the compounds. In the spectrum of the porphyrin Schiff base ligand (L), the molecular ion peak $[M+H]^+$ was shown at m/z= 1402.66 as a main peak. On the other hand, the Cu(II), Fe(III) and Zn(II) complexes show the molecular ion peaks at m/z= 1757.15, 1724.54 and 1765.08, respectively. In the MALDI-MS spectrum of the Pt(II) complex, the peak at m/z= 2284.57 may be assigned to the molecular ion $[M+H]^+$. In the spectrum of the Mn(III) complex, the molecular ion peak was not obsrved, instead, the peak at m/z= 1625.5 can be attributed to the $[C_{102}H_{70}Mn_2N_{10}O_5]^+$ ion. In the course of formation of this ion, the $[Mn(AcO)_2(H_2O]$ group from the main complex was seperated. The main peak at m/z= 1398.42 can be attributed to the free ligand $[M]^+$ ion.

Infrared spectral data of the TPP, TPP-NO_2, TPP-NH_2, L and transition metal complexes are given in the experimental section. As shown also from the spectral data, the FTIR absorption frequencies were different from free porphyrin Schiff base ligand and its metal complexes. It was found that the N-H bond stretching and bending frequencies of the TPP, TPP-NO_2, TPP-NH_2 and L located in the 3324-3311 cm^{-1} range and at ~964 cm^{-1}. In the spectra of the TPP, TPP-NO_2 and TPP-NH_2 compounds, the bands in the 2988-3021 cm^{-1} may be assigned to the C-H bond of the benzene and pyrrole rings. The bands in the 1494-1480 and 1344-1349 cm^{-1} range can be attributed to the C=C stretching mode and the C=N stretching vibration, respectively. In the spectrum of the free porphyrin Schiff base ligand, the stretching band at 1618 cm^{-1} can be attributed to the azomethine group. In the spectra of the complexes, the CH=N vibration were shown in the 1621-1610 cm^{-1} range and this situation shows that the nitrogen atom of the azomethine group coordinated to the metal ions. When the

metal ions were inserted into the porphyrin ring, the N-H bond vibration frequency (Fig. 6) of free base porphyrins disappeared and the characteristic Fe-N bond formed in the range of 1011-1002 cm^{-1}, which indicated the formation of iron porphyrin compounds [31]. The M-O and M-N band vibrations were shown in the 580-530 and 462-450 cm^{-1} range. The FAR characterization of M-Cl bond vibration (M: Cu(II), Fe(III), Pt(II) and Zn(II)) located at 357-374 cm^{-1}.

3.4 UV-Vis spectral properties

In order to determine the solvent effect, the electronic properties of the synthesized porphyrin based compounds were investigated in the DMSO, DMF, CH_2Cl_2 and toluene solutions. Obtained Uv-vis absorption spectral data of the TPP and TPP-NO_2 compounds are given in the experimental section. The electronic absorption spectral data and the molar extinction coefficients of the TPP-NH_2, porphyrin Schiff base ligand (L) and its transition metal complexes are given in Table 2. The UV-vis spectra of the TPP-NH_2, porphyrin Schiff base ligand and its transition metal complexes in the DMF solution are given in Fig. 7. As shown also from obtained data, the UV–vis spectra of TPP and TPP-NO_2 compounds showed the bands centered at 416, 418 nm (Soret band), and four Q bands absorptions in the 515- 648 and 514-646 nm range, respectively. It could also be observed that the absorption band in the UV-vis region of free porphyrin compound with –NO_2 group at 418 nm, which revealed the red shift compared to free TPP compound (2 nm). The reason might be that the strong electron-withdrawing –NO_2 group decreased the electronic density of the porphyrin ring. Thus, the energy levels of π_1 and π_2 orbits were increased and the energy gap between HOMO and LUMO of the porphyrin ring became smaller. The π-π^* electron excitation of the porphyrin ring required absorbing the light of smaller energy (longer wavelength), accordingly the absorption band (Soret band) occurred red shift and located in the long wavelength region. In the spectra of the TPP-NH_2 compound in different solutions, the Soret band were highly red shifted to 480 nm (~60 nm). Q bands of this compound are four pieces and these bands were observed in the 517-652 nm range. In the spectrum of the porphyrin Schiff base ligand, one Soret band and four weak Q bands were observed. The ligand, aside from Soret and Q bands, a new absorption band at 379 nm appeared can be attributed to the π-π^* transitions of the azomethine group. The absorption spectra of the porphyrins do not show n- π^* transitions owing to the symmetry of the n-orbitals and asymmetry of the π-orbitals in point of the plane of the porphyrin compound.

Soret bands shifted to the lower wavenumbers in the 478-483 nm range in DMSO, DMF, CH_2Cl_2 and toluene solutions. This red shift is owing to the hyperconjugation on the porphyrin Schiff base molecule by the π electron delocalization. On the other hand, Q bands were shown in the 514-649 nm range. The relative intensities of Q bands are in order of IV > III > II > I. This situation is consistent with the literature data [32].

The interference of Cu(II), Fe(III), Mn(III), Pt(II) and Zn(II) metal ions into the porphyrin ring caused blue- or red-shift of ~3-5 nm of the related Soret band as well as a decreasing number of Q bands in their UV–vis spectra. This is because when the hydrogen ions of N-H was replaced by the metal ions, the symmetry of the porphyrin ring increases. In the UV-vis spectra of the LCu_4Cl_3 complex in the different solvents, Q band at ~516 nm disappeared and other three bands at 539, 540 and 541 nm shifted to shorter wavelenghts compared to the ligand (L). Soret bands of the complexes shifted to the shorter wavenumbers (413-483 nm range). Q bands of the complexes were shown in the 503-684 nm range. Quantity of the Q bands were determined as two, three or four in the transition metal complexes and this situation is agreed with the literature data [33-36].

3.5 Photoluminescence properties

The photoluminescence properties of the ligand (L) and its metal complexes were investigated in DMF solution and different concentrations ($1.0x10^{-5}$-$1.0x10^{-7}$ M) at room temperature. The obtained data are given in Table 3a,b. The emission and excitation spectra of the compounds L and LCu_4Cl_3 were shown in Fig. 8. The excitation spectrum of the free ligand (L) shows one peak at 383 nm. Depending upon decreasing of the concentration, the intensity of the excitation peak decreases and shifts to the lower wavelenghts. The emission of the free porphyrin Schiff base ligand shows one strong peak at 659 nm, seems to be free porphyrin compound in different solvents [37]. One of them is S_2 (B band) and the other is S_1 (Q band). The fluorescence emission of the B (Soret) band is attributed to the transition from the second excited singlet state S_2 to the ground state S_0, $S_2 \rightarrow S_0$. The Soret emission band was about two orders of magnitude weaker than the $S_1 \rightarrow S_0$ transition of the Q band emission.

In the excitation spectra of the transition metal complexes, the Cu(II) and Fe(III) complexes showed one band at 356 nm in $1.0x10^{-3}$ M concentration. Against to the lower concentrations, the band at 356 nm shifted to the longer wavenumbers at 376 and 372 nm, respectively [38]. The Zn(II) complex indicates the excitation band. The band at 350 nm in

$1.0x10^{-3}$ M concentration shifted to 366 nm in the lower concentrations. In the excitation spectra of the Mn(III) and Pt(II) complexes, only one band at 352 and 397 nm was observed, respectively. In the lower concentrations, the band shifted to lower wavenumbers. Concentration differences have effect on the excitation spectra of the porphyrin Schiff base ligand and its transition metal complexes. On the other hand, ethyl group on the benzenoid ring has the electron donating property to the aromatic ring by the mesomeric and inductive effects. Electron-donating effect falled the energy difference between HOMO and LUMO, and cause λ shift to red direction.

In the emission spectrum of the Pt(II) complex, in $1.0x10^{-3}$ M solution, the a band with the high intensity at 641 nm was shown, and this band shifted to the lower wavenumber (650 nm) in the $1.0x10^{-7}$ M solution. While the Mn(III) complex showed the emission band at 673 nm in $1.0x10^{-3}$ M concentration, the Cu(II), Zn(II) and Fe(III) complexes indicated the bands at 704, 667 and 617 nm, respectively. The emission band of the Cu(II) complex shifted to lower wavelenght than the other complexes. Other emission bands show blue shift to 617 nm. On the other hand, the emission band of the Fe(III) complex also shifted to the blue region.

3.6 Thermal properties

Thermal stabilities of the ligand and its metal complexes were studied in the 20-1000 °C temperature range under N_2 atmosphere. The Cu(II) complex begins to decompose at 90 °C, and this mass loss may be attributed to the adsorbed water molecules. About 3.93% of the mass has been lost. In the first decomposition process, the Fe(III) and Mn(III) complexes showed the mass lost at about 120 °C and this can be attributed to the coordinated water molecules. In the 200-300 °C temperature range, coordinated chloride ions, except the Mn(III) complex, move away from the structures [39]. In this step, about 8.50% of the mass of the complexes was lost. In the Mn(III) complex, coordinated acetate ions were removed at about 280 °C temperature. At this temperature, the mass loss of the complex corresponds to 13.76% of total mass. The subsequent decomposition of the Pt(II), Fe(III) and Mn(III) complexes start at about 405 °C, and continue up to 850 °C. On the other hand, the last decomposition of the Cu(II) and Zn(II) complexes begins at 470 °C and continues up to 1000 °C. After the organic moiety (L) of the complexes decomposed, the metal oxides (CuO, ZnO, Fe_2O_3, PtO and Mn_2O_3) formed at higher temperatures. The Cu(II) and Zn(II) complexes have the higher thermal stability than the other complexes. Order of thermal stability is Cu(II) > Zn(II) > Pt(II) > Fe(III) > Mn(III).

3.7 Electrochemical properties

Electrochemical properties of the porphyrin Schiff base ligand and its metal complexes were investigated in DMF-0.1 M Bu_4NBF_4 as supporting electrolyte at 293 K. All potentials quoted refer to measurements run at a scan rates in the 100–1000 mVs^{-1} range and against an internal ferrocene–ferrocenium standard, unless otherwise stated. The electrochemical studies were studied in the 1 x 10^{-3} and 1 x 10^{-4} M DMF solutions and obtained data are given in supplementray file. The cyclic voltammograms of the ligand L (a) and its Pt(II) (b) complex are shown in Fig. 9. The voltammograms were recorded in the range from -2.0 to 2.0 V vs Ag^{+}/AgCl. In $1x10^{-3}$ M DMF solution, the free porphyrin Schiff base ligand (L) has the two anodic peak potentials in the -0.74-0.54 V range at 100-1000 mV/s scan rates. In addition, the ligand has one anodic peak in the -0.11-(-0.15) V range. On the other hand, in $1x10^{-4}$ M DMF solution, the ligand has two anodic and cathodic peaks in the -054-0.39 V and -1.24-(-0.29) V range, respectively, at all scan rates. In these concentrations, all redox processes are irreversible for free ligand. In $1x10^{-3}$ M DMF solution, the Cu(II) complex shows the reversible redox processes at 0.27/0.28 V, 0.28/0.29 V, 0.29/0.30 V, 0.30/0.31 V and 0.31/0.32 V couples, respectively. But, in $1.0x10^{-4}$ M DMF solution, the complex has two anodic and cathodic peaks in the -0.54-0.39 and -1.24-(-0.29) V, respectively, and these redox processes are irreversible. In $1x10^{-3}$ M DMF solution, the Pt(II) complex has quasi-reversible redox processes in the 0.55-0.74 V (E_{pa}-E_{pc}) range. In $1x10^{-4}$ M DMF solution, the Pt(II) complex has irreversible redox processes in the 0.10-0.79 V range. The Zn(II) complex shows irreversible redox processes in the $1.0x10^{-3}$ M solution, however these redox processes became reversible in the $1.0x10^{-4}$ M solution at all scan rates. The Fe(III) and Mn(III) complexes indicate one or two anodic and cathodic peak potentials in the -0.60-0.67 and -1.04-0.79 V, respectively and these processes are irreversible. By the increasing of the scan rate, while the cathodic peak potentials shifted to the negative regions, the anodic peaks were shifted to the more possitive regions. When the concentration of the solution of the ligands decreases to $1x10^{-4}$ M, the anodic and cathodic peak potentials data were both reduced and increased.

3.8 SOD Activity studies

Measuring SOD activity is rather difficult, since the $O_2^{\cdot -}$ free radical has a short half-life in neutral aqueous solution. There are many direct and indirect methods reported for

measuring the SOD activity. The direct measurement of SOD activity falls into two categories: stopped-flow kinetic analysis and pulse radiolysis [40]. Cyctochrome c and nitrobluetetrazolium (NBT) are the most commonly used redox indicators due to their convenience and ease of use [41,42]. In these methods, xanthine/xanthine oxidase generates steady-state low levels of superoxide. On the other hand, NBT has some disadvantages such as poor water solubility of the formazan dye and the interaction with the reduced form of xanthine oxidase.

The SOD activity of porphyrine Schiff base metal complexes were evaluated by a modified indirect chemical method [43]. The results of our complexes and some literature data are shown in Table 4. The SOD test results indicated that these compounds could be considered as good SOD-mimics, as compared with native bovine Cu, Zn-SOD and some related complexes listed in Table 4. The SOD activity of the Mn^{3+}, Fe^{3+}, Zn^{2+} and Pt^{2+} are similar IC_{50} values and slightly higher than that of Cu^{2+} complex. The dismutation of superoxide to molecular oxygen and hydrogen peroxide by the complexes is shown in the equation below.

$$2O_2^{\cdot -} + 2H^+ \xrightarrow{\text{Complex}} O_2 + H_2O_2$$

Direct comparisons of SOD activity of complexes with other related complexes are somewhat complicated due to diverse methodology used for the formation of superoxide. Acoording to IC50 values, the complexes exhibit lower activity than Cu/ZnSOD (native bovine) [43] and manganese porphyrine complex $[MnTM\text{-}4\text{-}PyP]Cl_5$ [44]. However, the manganese salen complex (EUK-8) [45,46] shows similar IC50 value to the complexes tested in this study.

3.9 DNA binding properties

The porphyrins and their metal complexes are known to bind to DNA *via* both covalent and/or non-covalent interactions [47]. In covalent binding, the labile porphyrin part of the complexes is replaced by a nitrogen base of DNA such as guanine N_7. Moreover, the non-covalent DNA interactions include intercalative, electrostatic and groove (surface) binding of compounds along outside of DNA helix, along major or minor groove. It has been reported that FSdsDNA can provide three distinctive binding sites for all compounds; namely, groove binding, electrostatic binding to phosphate group and intercalation [48]. This behavior is of great importance with regard to the relevant biological role of porphyrins and metallo

porphyrins in the body. The interaction can be studied with UV spectroscopy in order to investigate the possible binding modes to FSdsDNA. The changes observed in the UV spectra upon titration may give the evidence of the existing interaction mode, since a hypochromism, due to π-π* stacking interactions, may appear in the case of the intercalative binding mode, while red-shift may be observed when the DNA duplex is stabilized. In UV titration experiments, the spectra of FSdsDNA in the presence of each compounds have been recorded for a constant compounds concentration in diverse [ligand or complex]/[FSDSDNA] mixing ratios (r). Fig. 10 shows the spectral changes occurred in $1x10^{-6}$ M methanolic solution of the ligand (L) upon addition of increasing amounts of FSdsDNA. Even though no appreciable change in the position of the intraligand band of the ligand (L) and its metal complexes are observed by addition of different initial concentration of FSdsDNA (0.4 ppm for L, 0.5 ppm for LCu_4Cl_3 and LZn_4Cl_3 and 1 ppm for LPt_4Cl_3). The intensity of the band centred at 415.7 nm for the ligand (L) (from 415.7 to 421.6 for L (A_{max}, from 0.63 to 0.24), from 413.2 to 419.9 for LCu_4Cl_3 (A_{max}, from 1.29 to 0.52), from 432.05 to 434.1 for $LZn4Cl_3$ (A_{max}, from 0.3 to 0.25) and from 416.1 to 422.5 for LPt_4Cl_3 (Λ_{max}, from 0.43 to 0.19) decreased in the presence of DNA. Upon increasing DNA concentration, the absortion intensity is increased for the ligand (L) over again. In general, the hyperchromism and hypochromism shifts are the spectral features of DNA concerning changes of its double helix structure. The hyperchromism means the breakage of the secondary structure of DNA. The hypochromism shows that binding of complex to DNA can be due electrostatic effect or intercalation which may stabilize the DNA duplex. Additionally, the existence of a red-shift is indicative of stabilization of DNA duplex [48]. On the other hand, addition of FSdSDNA to the ligand (L) results in slight hypochromism of the band at λ_{max}= 415.7 nm, which is accompanied by a red-shift of 5.9 nm (up to 421.6 nm). These spectral changes may be evidence of a possible intercalation, which could subsequently stabilize the DNA duplex [49]. For all complexes, the band centered at 413.2, 432.05 and 416.1 nm exhibits a less pronounced chromism of 40.31 % for copper complex, 83.33 % for zinc complex and 44.20% for the platinium complex upon addition of FSdsDNA accompanied with a red-shift (Fig. 11). The binding strength of the ligand (L) and its complexes with FSdsDNA is mirrored in the intrinsic binding constant K_b, which represents the binding constant per DNA base pair and can be obtained by monitoring the changes in the absorbance at different wavelenghts (for all compounds) with increasing concentrations of FSdsDNA, according to the following equation (Eq. 1) [50,51]:

$$[DNA] / (\varepsilon_a - \varepsilon_f) = [DNA] / (\varepsilon_b - \varepsilon_f) + 1 / K_b(\varepsilon_a - \varepsilon_f) \qquad \text{(Eq. 1)}$$

where $\varepsilon_a = A_{obs}$ / [Complex], ε_a = extinction coefficient for the free complex and ε_b = extinction coefficient for compound in the fully bound form, respectively. In plots [DNA] / ($\varepsilon_b - \varepsilon_f$) versus [DNA], K_b is given by the ratio of slope to the y intercept (insets in Figs. 10&11). The determined K_b values for the ligand (L) and its metal complexes are given in Table 5. The high value of K_b obtained for LPt_4Cl_3, LCu_4Cl_3 or ligand (L), and LZn_4Cl_3 suggest a strong binding of complexes to FSdsDNA. Indeed, it is much higher than K_b calculated for the ligand (L), indicating that the coordination of porphyrin ligand (L) to M(II) ion enhance significantly the ability to bind to FSdsDNA. This is an important point. The K_b values of the porphyrin Schiff base ligand (L) and its metal complexes are higher than the EB binding affinity for DNA ($K_b = 1.23 \pm 0.07 \times 10^5$). For the reason that, the intercalative interaction may affect EB displacement [52,53]. In addition, a distinct isosbestic point appears at about 425.1 nm upon addition of FSdsDNA. The behavior of complexes upon addition of FSdsDNA is quite similar.

Conclusion

In this study, a new symmetric porphyrine-Schiff base ligand and its transition metal complexes were synthesized and chracterized by spectroscopic and analytical methods. Starting compounds 4-ethyl-2,6-bis(hydroxymethyl)phenol and 4-ethyl-2,6-diformylphenol were obtained as single crystals and their structures were identified by X-ray crystallography method. Uv-Vis, emission, excitation, electrochemical and thermal properties of the ligand and its metal complexes were investigated in detail. Superoxide dismutase activities of the porphyrin Schiff base metal complexes were investigated. In addition, the study of the porphyrin and metalloporphyrin interaction with FSdsDNA has been performed with UV spectroscopy and it reveals that the complexes can bind to DNA. The UV spectroscopic titrations were used in order to calculate the binding strength of the complexes with FSdsDNA which is mirrored in the intrinsic binding constant K_b. The LPt_4Cl_3 complex exhibits much higher intrinsic binding constant to FSdsDNA than the other complexes, porphyrin ligand and EB.

Supplementary Information

CCDC numbers 1038663 and 1038664 contain the supplementary crystallographic data for (A) and (B), respectively. Bond lenghts and angles of the compounds were given in Supplementary Information. These data can be obtained free of charge *via*

www.ccdc.cam.ac.uk/data_request/cif, by e-mailing data_request@ccdc.cam.ac.uk, or by contacting The Cambridge Crystallographic Data Centre 12 Union Road Cambridge CB2 1EZ, UK Fax: +44(0)1223-336033.

Acknowledgments

We are grateful to The Scientific & Technological Research Council of Turkey (TUBITAK) (Project number: 113Z907) for the support of this research. The authors are also grateful to the Department of Chemistry, Loughborough University for X-ray data collection.

References

[1] A.R. Battersby, Pure Appl Chem, 65 (1993) 1113-1122.

[2] K.M. Kadish, K.M. Smith, R. Guilard (Eds.), The Porphyrin Handbook, vols. 1–10, Elsevier Science, Oxford, 2000.

[3] B. Kräutler, Chimia, 41 (1987) 277-292.

[4] K.M. Kadish, K.M. Smith, R. Guilard (Eds.), The Porphyrin Handbook, vols. 11–20, Elsevier Science, Oxford, 2000.

[5] J. Stehr, J.M. Lupton, M. Reufer, G. Raschke, T.A. Klar, J. Feldmann, Adv Mater., 16 (2004) 2170–2174.

[6] D.V. Rao, F.J. Aranda, J.F. Roach, D.E. Remy, Appl Phys Lett, 58 (1991) 1241-1243.

[7] P.K. Poddutoori, B.G. Maiya, Indian J Chem A, 42 (2002) 2198-2204.

[8] D.M. Li, Z.X. Zhao, S.Q. Liu, G.F. Liu, T.S. Shi, X.X. Liu, Synth. Commun, 30 (2000) 4017-4026.

[9] R.J. Fiel, J Biomol Str Dyn, 6 (1989) 1259-1275.

[10] R.J. Fiel, J.C. Howard, E.H. Mark, N.D.Gupta, Nucleic Acids Res., 15 (1979) 6553-6562.

[11] R.F. Pasternack, E.J. Gibbs, J.J.Villafranca, Biochemistry, 22 (1983) 2406-2414.

[12] K. Ford, K.R. Fox, S. Neidle, M.J.Waring, Nucleic Acids Res., 15 (1987) 2221-2234.

[13] S.D. Bromley, B.W. Ward, J.C. Dabrowiack, Nucleic Acids Res., 14 (1986) 9133-9148.

[14] T.N.Sorrel, Jpn J Cancer Res., 90 (1999) 555-564.

[16] Y. Kobayashi, K. Kariya, K. Saigenji, K. Nakamura, Cancer Biother., 9 (1994) 171-178.

[17] X.M. Yin, Z. Dong, Totowa, New Jersey (2003).

[18] Bruker (1998). APEX2 and SAINT Bruker AXS Inc.

[19] G.M. Sheldrick, Acta Cryst, A64 (2008) 112-122.

[20] G.H. Barnett, M.F. Hudson, K.M. Smith, J Chem Soc Perkin Trans, 1 (1975) 1401-1403.

[21] W.J. Kruper, J.A. Chamberlin, M. Kochanny, J Org Chem, 54 (1989) 2753-2756.

[22] R. Luguya, L. Jaquinod, F. R. Fronczek, M. Graça, H. Vicente, K. M. Smith, Tetrahedron, 60 (2004) 2757-2763.

[23] J.M. Mccord, I. Fridovic, J Biol Chem., 244 (1969) 6049-6055.

[24] H. Muslu, A. Golcu, S.A. Ozkan,. Curr. Anal. Chem. 6 (2010) 299-309.

[25] B. Masci, P. Acta Cryst, C58 (2002) o575-579.

[26] D. Oehler, A. Thozet, M. Perrin, Acta Cryst, C41 (1985) 1766-1768.

[27] Z.L. Chu, W. Huang, S.H. Gou, Acta Cryst, E61 (2005) o1624-1625.

[28] J.C. Jiang, G. Wang, W. You, W. Huang, Acta Cryst, E64 (2008) o1426-1427.

[29] S. Duclos, B. Therrien, T.R.Ward, Acta Cryst, E57 (2001) o884-885

[30] K. Rajesh, A.K. Rahiman, K.S. Bharathi, S. Sreedaran, V. Gangadevi, V. Narayanan, Bull Korean Chem Soc, 31(9) (2010) 2656-2664.

[31] W. Lian, Y. Sun, B. Wang, N. Shan, T. Shi, J Serb Chem Soc, 77(3) (2012) 335–348.

[32] L.J. Prins, D.N. Reinhoudt, P. Timmerman, Angew. Chem Int Ed, 40 (2001) 2382-2426.

[33] C.W. Huang, K.Y. Chiu, S.H. Cheng, Dalton Trans, (2005) 2417–2422.

[34] Y. Huang, "Synthesis and Reduction of Iron(III) Porphinone Complexes and Their Spectroscopy Studies", Master's Theses 2009: 1-90.

[35] S. Cai, E. Belikova, L.A. Yatsunyk, A.M. Stolzenberg, F.A. Walker, Inorg. Chem., 44 (2005) 1882-1889.

[36] S. Dubey, G.D. Bajju, R. Javed, T. Sadiq, Indian J Chem, 47A (2008) 529-534.

[37] J.L. Retsek, C.J. Medforth, D.J. Nurco, S. Gentemann, V.S. Chirvony, K.M. Smith, D. Holten, J Phys Chem B, 105 (2001) 6396-6411.

[38] Z. Wang, K.J. Ho, C.J. Medforth, J.A.Shelnutt, Adv Matter, 18 (2006) 2557–2560.

[39] M. Dolaz, V. McKee, S. Uruş, N. Demir, A.E. Şabik, A. Gölcü, M. Tümer, Spectrochim. Acta Part A, 76(2) (2010) 174–181.

[40] D. Riley, Chem. Rev., 99 (1999) 2573-2587.

[41] S. Goldstein, G. Czapski, Free Radic. Res. Commun., 12(3) (1991) 5-10.

[42] S. Goldstein, G. Czapski In Free Radicals, Eds. P. Neville and K. Frank, Oxford University Press, Oxford, (1996) 241-255.

[43] J. J. Vanco, O. Svajlenova, E. Racanska, J. Muselık, J. Valentova, Journal of Trace Elements in Medicine and Biology, 18(2) (2004) 155–161.

[44] I. Spasojevic, I. Batinic-Haberle, R.D. Stevens, P. Hambright, A.N. Thorpe, J. Grodkowski, P. Neta, I. Fridovich, Inorg. Chem., 40 (2001) 726–739.

[45] M. Baudry, S. Etienne, A. Bruce, M. Palucki, E. Jacobsen, B. Malfroy, Biochem. Biophys. Res. Commun., 192 (1993) 964–968.

[46] I. Batinic-Haberle, L. Benov, I. Spasojevic, I. Fridovich, J. Biol. Chem., 273 (1998) 24521–24528.

[47] O.A. Kovaleva, V.B. Tsvetkov, O.K. Mamaeva, V.A. Ol'shevskaya, A.V. Makarenkov, L.G. Dezhenkova, A.V. Makarenkov, L.G. Dezhenkova, A.S. Semeikin, O.F. Borisova, A.A. Shtil, A.K. Shchyolkina, D. N. Kaluzhny, European Biophysics Journal With Biophysics Letters, 43(10-11) (2014) 545-554.

[48] P. Christofis, M. Katsarou, A. Papakyriakou, Y. Sanakis, N. Katsaros, G. Psomas, J of Inorg. Biochem., 99 (11) (2005) 2197-210.

[49] N. Demirezen, D. Tarınç, D. Polat, M. Çeşme, A. Gölcü, M. Tümer, Spectrochim. Acta Part A, 94 (2012) 243-55.

[50] M. Çeşme, A. Gölcü, İ. Demirtaş, Spectrochim Acta Part A, 25(135) (2015) 887-906.

[51] G. Psomas, J of Inorg. Biochem, 102(9) (2008) 1798-1811.

[52] K. Gehring, J.L. Leroy, M. Gueron, Nature, 363(6429) (1993) 561-565.

[53] R. Paolesse, D. Monti, S. Nardis, C. Di Natale, Porphyrin-based chemical sensors. In: K.M. Kadish, K.M. Smith, R. Guilard (eds) Handbook of porphyrin science 2010; vol. 12, Chapter 54. World Scientific, Singapore, p. 121

Table 1

Crystallographic data for the starting materials A and B.

Identification code		**A**	**B**
Empirical formula		$C_{10}H_{14}O_3$	$C_{10}H_{10}O_3$
Formula weight		182.21	178.18
Crystal size (mm^3)		0.41 x 0.36 x 0.08	$0.31 \times 0.23 \times 0.10$
Crystal color		colourless	Yellow
Crystal system		*Monoclinic*	*Triclinic*
Space group		*P2(1)/c*	*P* $\bar{1}$
Unit cell	a (Å)	16.3457(16)	7.6563(6)
	b (Å)	13.3873(13)	7.8598(7)
	c (Å)	8.3694(8)	8.4085(7)
	α (°)	90	73.2310(10)
	β (°)	94.5084(15)	71.0790(10)
	γ (°)	90	66.6050(10)
Volume (Å3)		1825.8(3)	431.81(6)
Z		8	2
Abs. coeff. (mm^{-1})		0.097	0.101
Refl. Collected		18678	5837
Completeness to θ = 28.10°		100%	99.6%
Ind. Refl. [R_{int}]		4535 [0.0330]	2105 [0.0201]
R1, wR2 [I>2σ (I)]		0.0408, 0.0981	0.0383, 0.1059
R1, wR2 (all data)		0.0534, 0.1076	0.0468, 0.1127
CCDC number		1038663	1038664

Table 2

Hydrogen-bond geometry (Å, °) for the starting compound (A).

D—H···*A*	*D*—H	H···*A*	*D*···*A*	*D*—H···*A*
O2—H1A···O3	0.878 (19)	1.878 (19)	2.6508 (12)	145.8 (16)
O2—H1A···O3^{i}	0.878 (19)	2.400 (18)	2.9764 (12)	123.5 (15)
C7—H7···O1^{ii}	0.95	2.65	3.5230 (14)	153.0
C10—H10···O1^{ii}	0.95	2.60	3.4834 (15)	154.5

Symmetry codes: (i) −*x*+1, −*y*, −*z*+2; (ii) *x*+1, *y*−1, *z*.

Table 3

Hydrogen bonds for the starting compound (B) [Å and °].

D—H···*A*	*D*—H	H···*A*	*D*···*A*	*D*—H···*A*
O(1)-H(1)...O(3)^{i}	0.824(18)	2.000(19)	2.8179(14)	171.5(17)
O(2)-H(2)...O(1)^{ii}	0.831(18)	1.905(18)	2.7043(13)	160.9(16)
O(3)-H(3A)...O(2)^{iii}	0.836(19)	2.025(19)	2.8610(14)	177.6(17)
O(4)-H(4)...O(5)^{iv}	0.90(2)	1.92(2)	2.7609(14)	156.4(18)
O(5)-H(5)...O(6)^{v}	0.901(19)	1.747(19)	2.6277(14)	165.0(17)
O(6)-H(6)...O(4)^{vi}	0.882(19)	1.821(19)	2.6907(14)	168.4(17)

Symmetry codes: (i) -x+1,-y+2,-z (ii) -x+1,-y+2,-z+1 (iii) x,-y+3/2,z-1/2 (iv) -x,-y+1,-z+1 (v) x,-y+1/2,z+1/2 (vi) -x,-y+1,-z

Table 4

UV-vis absorption spectral data of ATTP-NH_2, the porphyrin Schiff base ligand (L) and its metal complexes in the different solvents (λ_{max} (nm) (ε_{max}, $M^{-1}cm^{-1}$)).

Compounds	DMSO	DMF	Toluene	CH_2Cl_2
ATTP-NH_2	479($1.28x10^4$),	481($0.47x10^4$),	425($3.34x10^4$),	481($0.58x10^4$),
	558($0.89x10^4$),	518($1.29x10^4$),	524($0.40x10^4$),	517($1.75x10^4$),
	592($1.01x10^4$),	557($0.93x10^4$),	560($0.30x10^4$),	554($1.01x10^4$),
	591($0.52x10^4$),	592($0.50x10^4$),	587($0.20x10^4$),	591($0.57x10^4$),
	652($0.50x10^4$)	651($0.51x10^4$)	650($0.10x10^4$)	649($0.58x10^4$)
L	478($0.90x10^4$),	379($0.50x10^4$),	483($0.77x10^4$),	482($0.84x10^4$),
	517($2.90x10^4$),	483($0.76x10^4$),	515($3.03x10^4$),	516($3.14x10^4$),
	546($1.89x10^4$),	514($2.28x10^4$),	553($1.71x10^4$),	552($1.76x10^4$),
	571($1.20x10^4$),	552($1.36x10^4$),	593($0.93x10^4$),	592($0.99x10^4$),
	641($1.03x10^4$)	592($0.74x10^4$),	649($0.76x10^4$)	645($0.86x10^4$)
		648($0.70x10^4$)		
LCu_4Cl_3	543($2.08x10^4$),	540($2.03x10^4$),	541($2.04x10^4$),	539($1.90x10^4$),
	585($0.69x10^4$),	585($0.50x10^4$),	580($0.37x10^4$),	578($0.43x10^4$),
	587($0.68x10^4$),	700($0.18x10^4$)	650($0.15x10^4$),	676($0.22x10^4$)
	659($0.12x10^4$)			
$LFe_3Cl_4(H_2O)$	521($1.95x10^4$),	516($2.17x10^4$),	516($1.42x10^4$),	503($3.02x10^4$),
	547($1.46x10^4$),	554($1.28x10^4$),	551($0.88x10^4$),	684($2.52x10^4$)
	588($0.72x10^4$)	653($0.65x10^4$)	590($0.67x10^4$)	
$LMn_3(ACO)_4(H_2O)$	516($2.42x10^4$),	463($3.22x10^4$),	475($3.52x10^4$),	476($3.30x10^4$),
	556($1.62x10^4$),	516($1.94x10^4$),	516($1.94x10^4$),	516($1.80x10^4$),
	592($1.19x10^4$)	554($1.12x10^4$),	552($1.19x10^4$),	552($1.11x10^4$),
		590($0.80x10^4$)	592($0.85x10^4$)	592($0.81x10^4$)
LPt_4Cl_3	516($2.42x10^4$),	463($3.22x10^4$),	475($3.52x10^4$),	476($3.30x10^4$),
	556($1.62x10^4$),	516($1.94x10^4$),	516($1.94x10^4$),	516($1.80x10^4$),
	592($1.19x10^4$)	554($1.12x10^4$),	552($1.19x10^4$),	552($1.11x10^4$),
		590($0.80x10^4$)	592($0.85x10^4$)	592($0.81x10^4$)
LZn_4Cl_3	518($1.85x10^4$),	478($1.71x10^4$),	484($0.52x10^4$),	549($1.92x10^4$),
	561($2.68x10^4$),	516($1.83x10^4$),	516($1.70x10^4$),	589($0.69x10^4$),
	602($1.61x10^4$)	559($2.68x10^4$),	556($2.07x10^4$),	680($0.78x10^4$)
		600($1.52x10^4$)	602($1.13x10^4$)	

Tables 5a,b.

Excitation (a) and emission (b) spectral data of the porphyrin Schiff base ligand and its transition metal complexes in the different concentrations.

a)	λ_{max} (nm)	Excitation			
Compounds	$1x10^{-3}$ (M)	$1x10^{-4}$ (M)	$1x10^{-5}$ (M)	$1x10^{-6}$ (M)	$1x10^{-7}$ (M)
L	383	381	380	379	377
LCu_4Cl_3	356	360	367	373	376
LZn_4Cl_3	350	353	357	360	366
LPt_4Cl_3	397	390	384	377	371
$LMn_3(AcO)_4(H_2O)$	352	350	347	343	340
$LFe_3Cl_4(H_2O)$	356	362	365	369	372

b)	λ_{max} (nm)	Emission			
Compounds	$1x10^{-3}$ (M)	$1x10^{-4}$ (M)	$1x10^{-5}$ (M)	$1x10^{-6}$ (M)	$1x10^{-7}$ (M)
L	659	655	648	642	638
LCu_4Cl_3	704	698	693	695	698
LZn_4Cl_3	667	665	663	661	659
LPt_4Cl_3	641	643	646	648	650
$LMn_3(AcO)_4(H_2O)$	673	670	665	661	657
$LFe_3Cl_4(H_2O)$	617	613	611	605	602

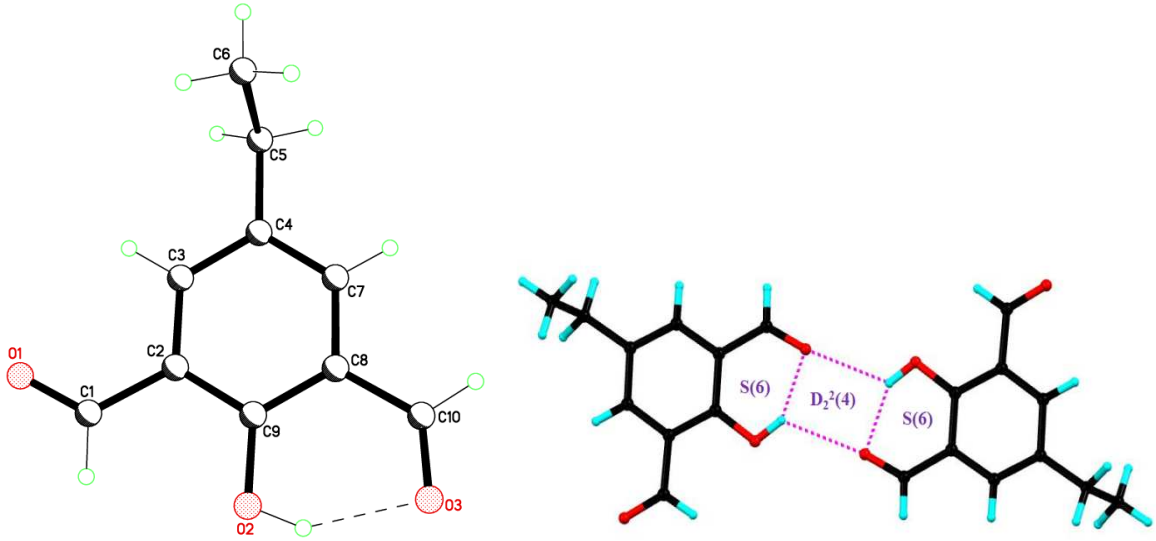

Fig. 1. Crystal structure of the starting compound (A) (left) and hydrogen bonded dimer (right).

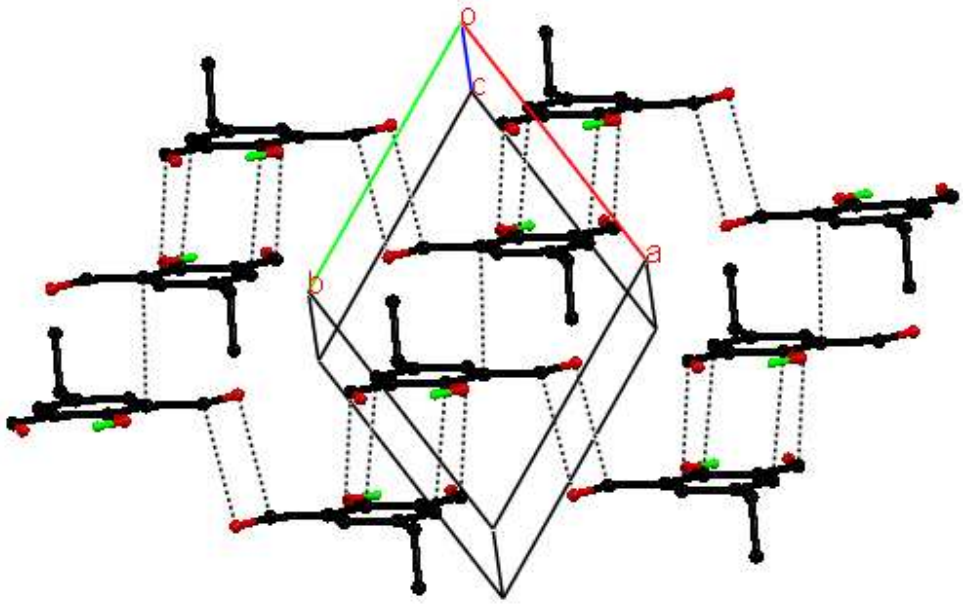

Fig. 2. Unit cell packing of the compound, π...π interactions shown as dashed lines, hydrogen atoms are omitted for clarity.

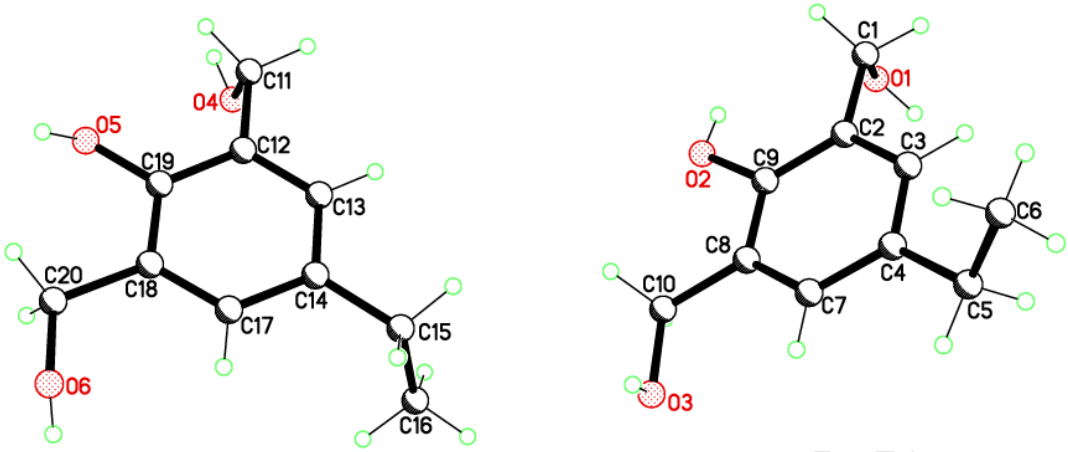

Fig. 3. The asymmetric unit of the starting compound (B) with atom numbering.

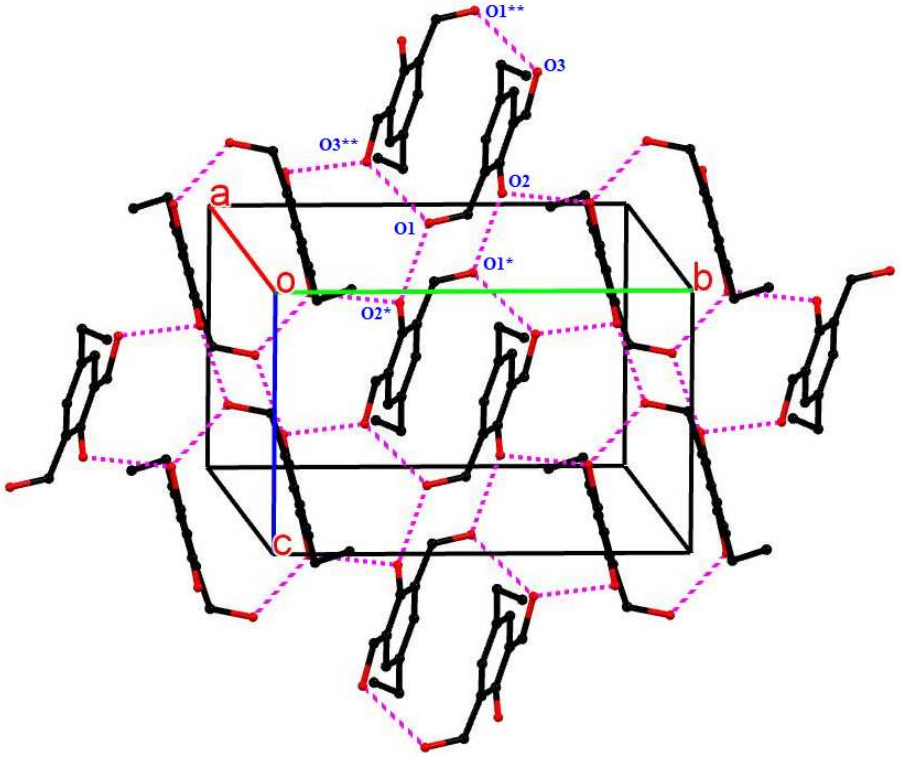

Fig. 4. Packing diagram of the starting compound (B) showing hydrogen bond network. Hydrogen atoms are omitted for clarity. Atom labels show centrosymmetric dimers held by two complementary hydrogen bonds. Symmetry codes: *:-x+1,-y+2,-z+1 **: -x+1,-y+2,-z

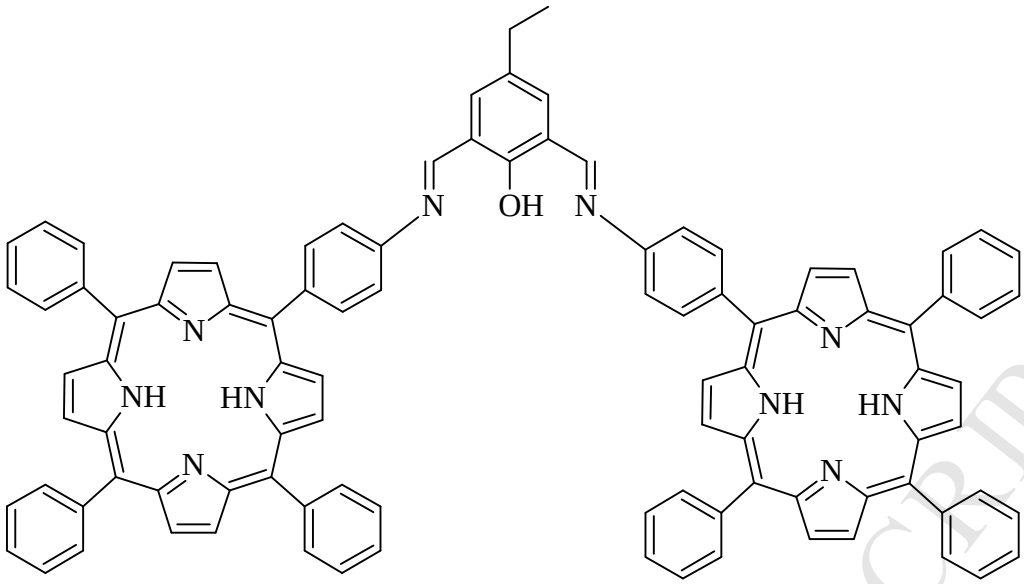

L

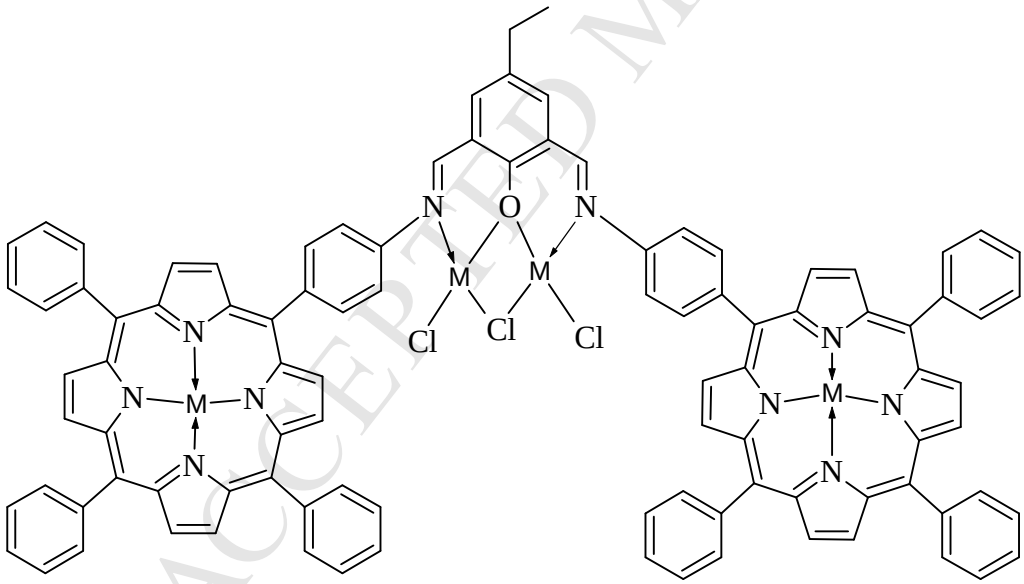

M: Cu(II), Pt(II) and Zn(II)

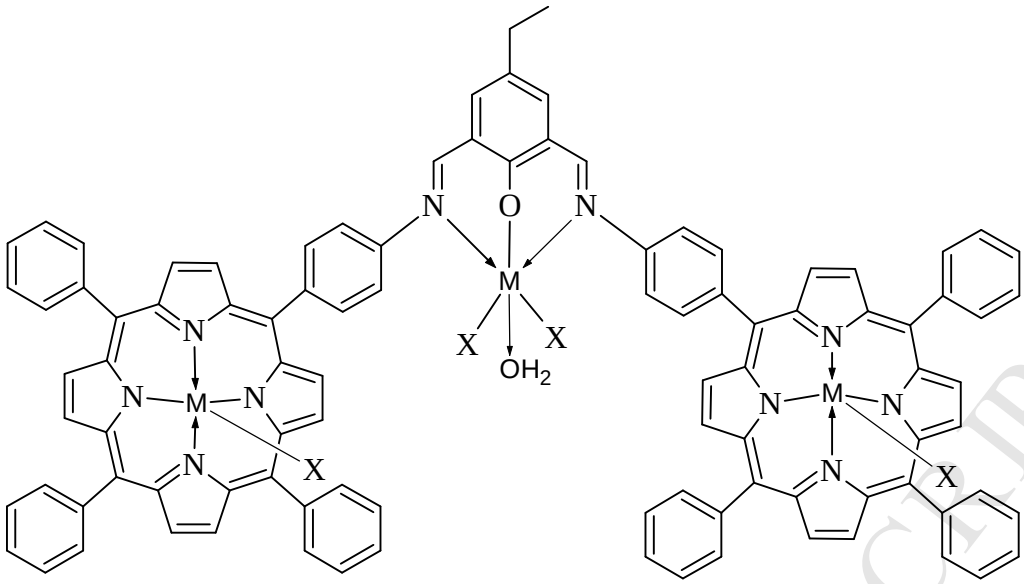

M: Fe(III) and Mn(III)

X: Cl^-, CH_3COO^-

Fig. 5. Proposed structures of the synthesized porphyrin Schiff base ligand and its complexes.

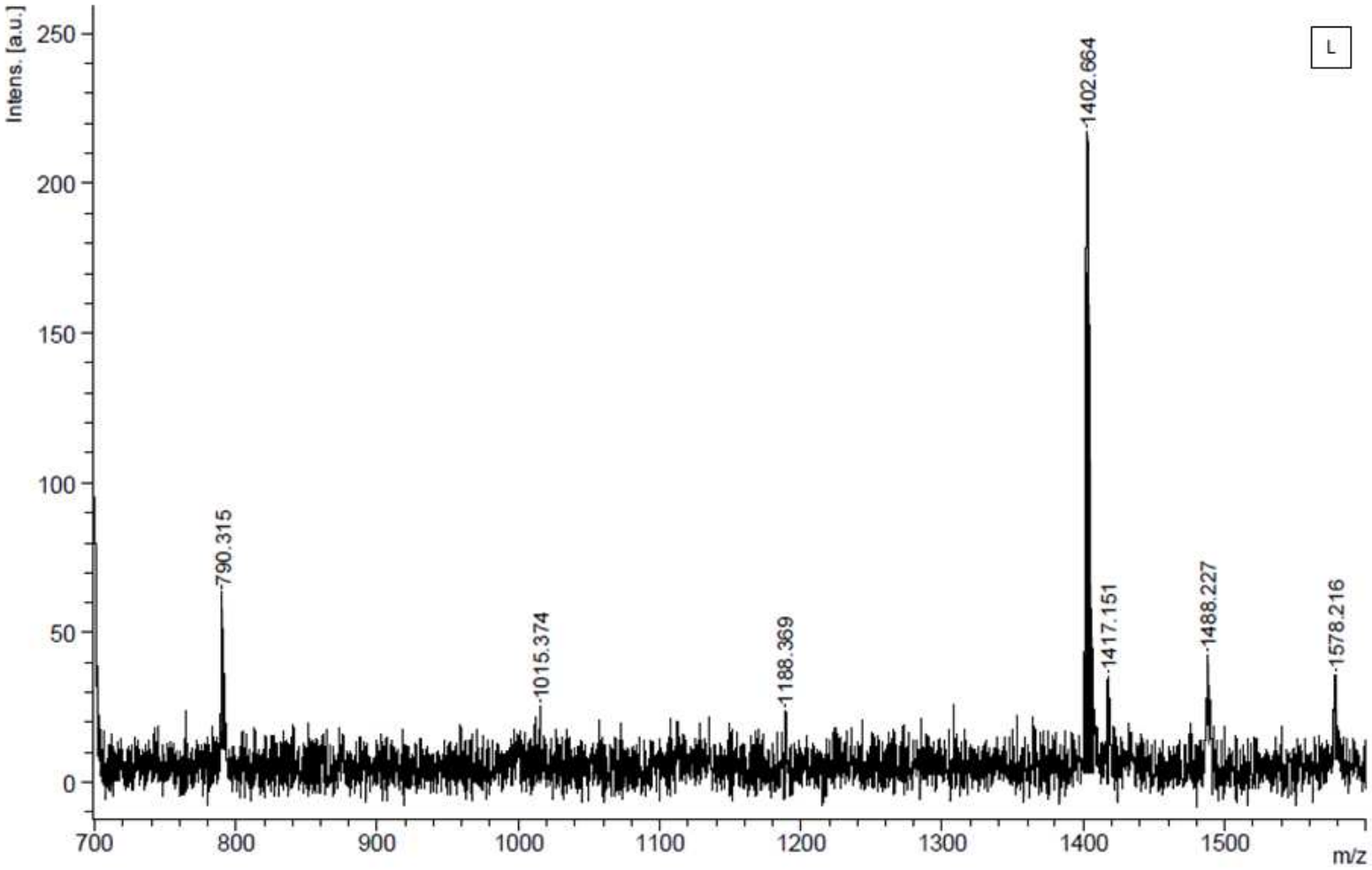

Fig. 6. MALDI- TOF mass spectrum of the porphyrin Schiff base ligand (HL).

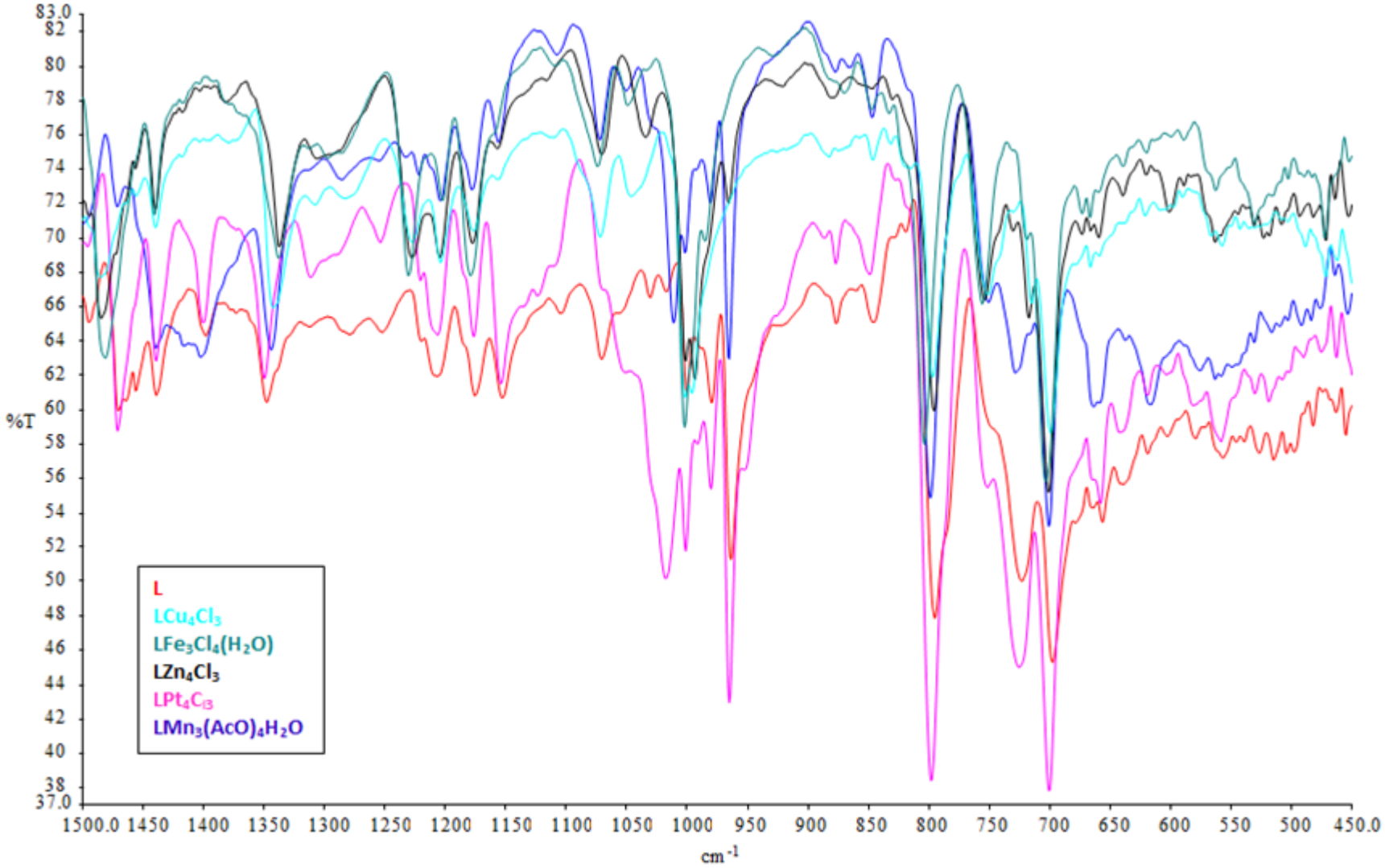

Fig. 7. FTIR spectra of the porphyrin Schiff base ligand (L) and its metal complexes.

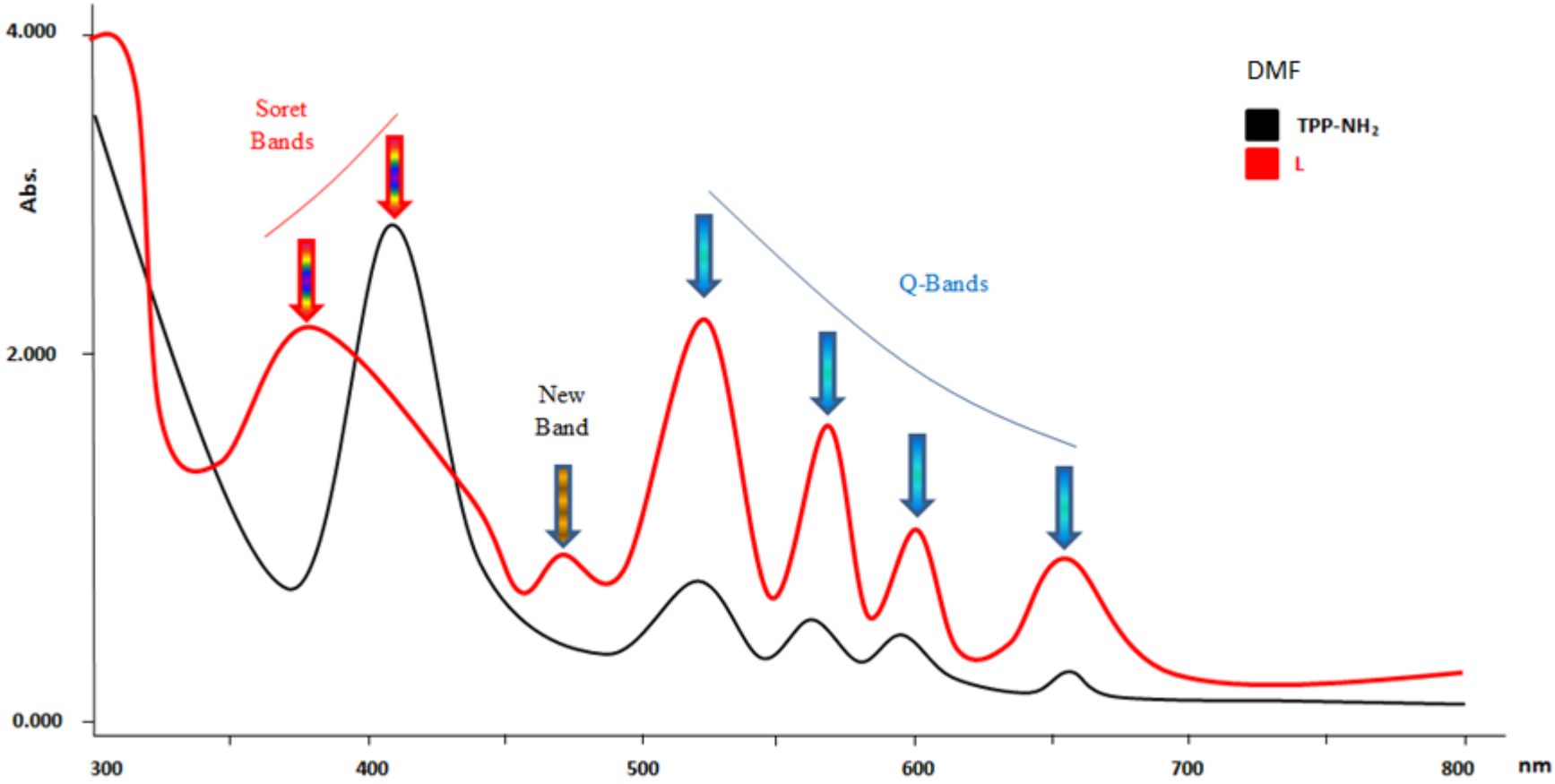
4.000
2.000
0.000
Abs.
300
400
500
600
700
800
nm
Soret
Bands
New
Band
Q-Bands
DMF
TPP-NH2
L

a)

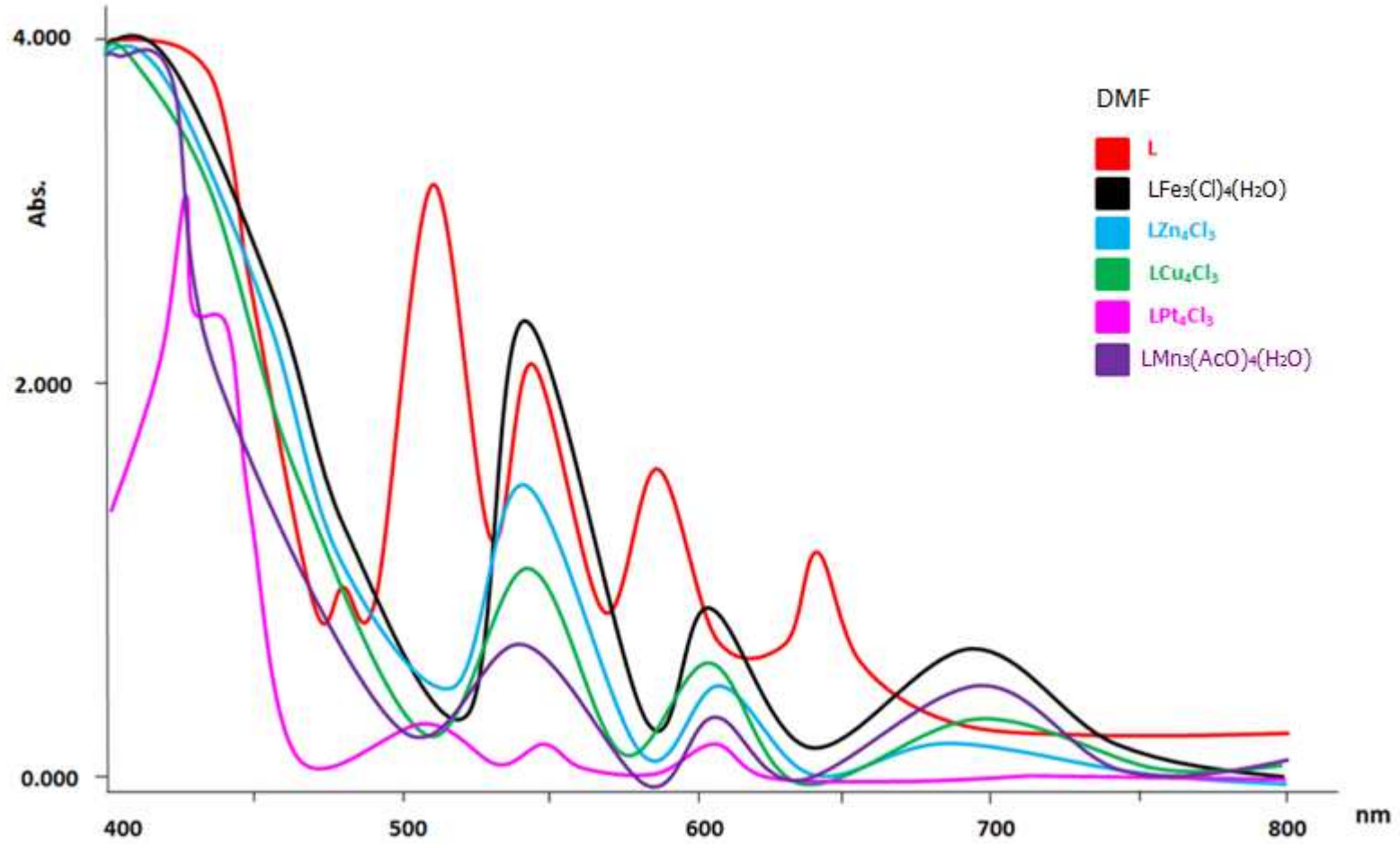

b)

Figs. 8a,b. Uv-vis absorption spectra of the TPP-NH_2, porphyrin Schiff base ligand (L) and its transition metal complexes in DMF solution.

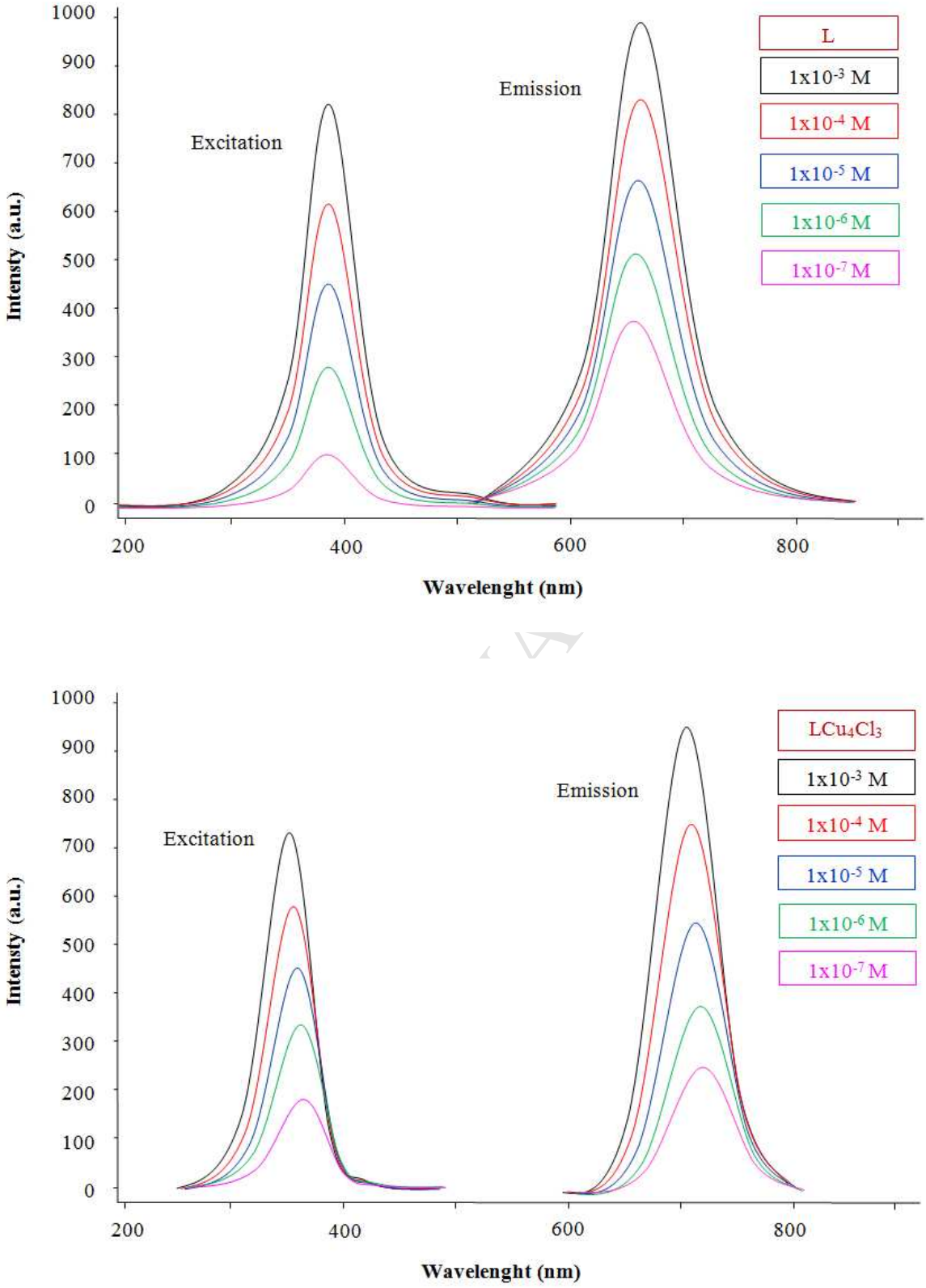

Fig. 9. Emission and excitation spectra of the ligand and its Cu(II) transition metal complex.

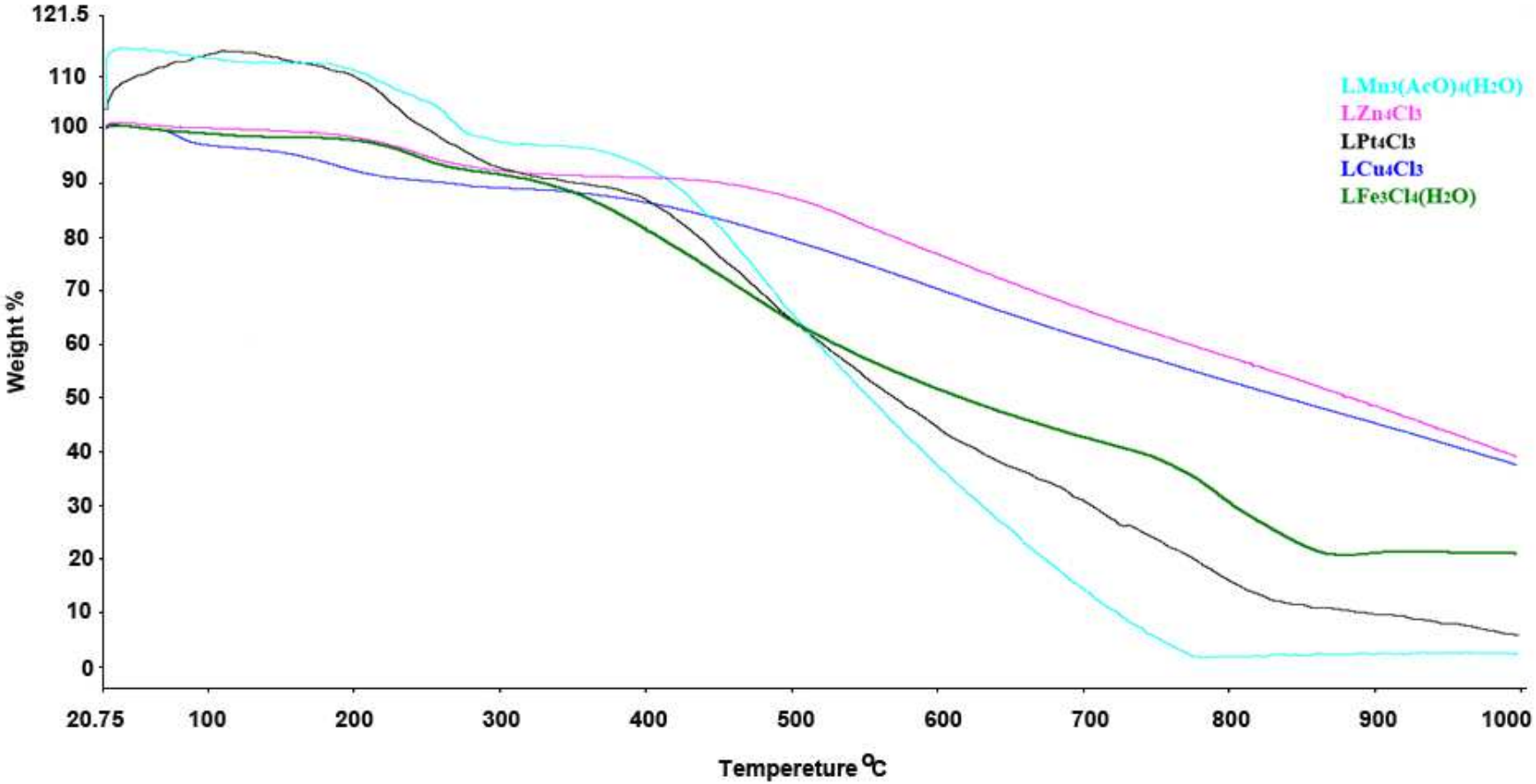

Fig. 10. TG curves of the porphyrin Schiff base complexes in the 20-1000 °C temperature range.

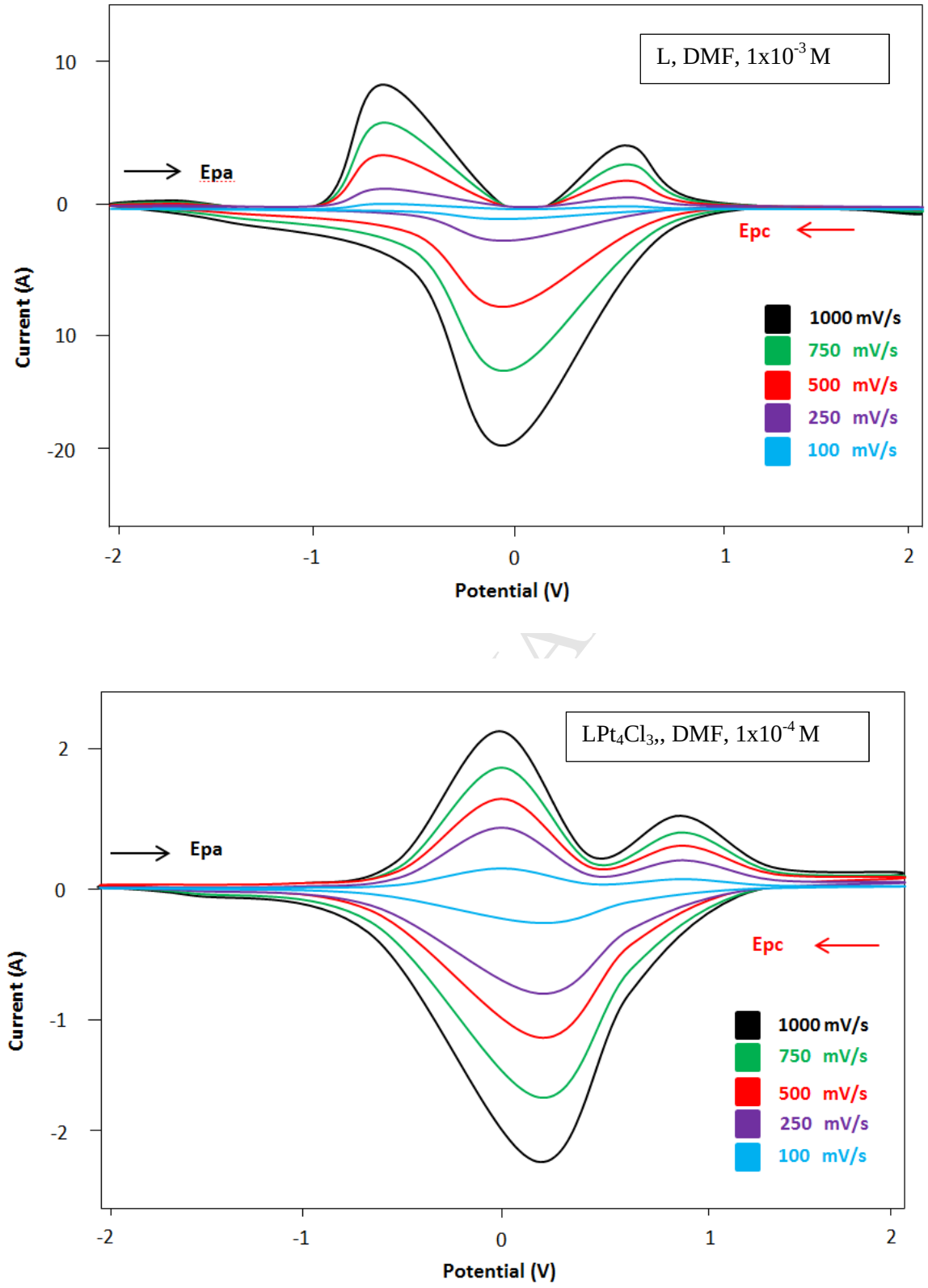

Fig. 11. CV curves of the ligand and its Pt(II) metal complex at different scan rates in DMF solution.

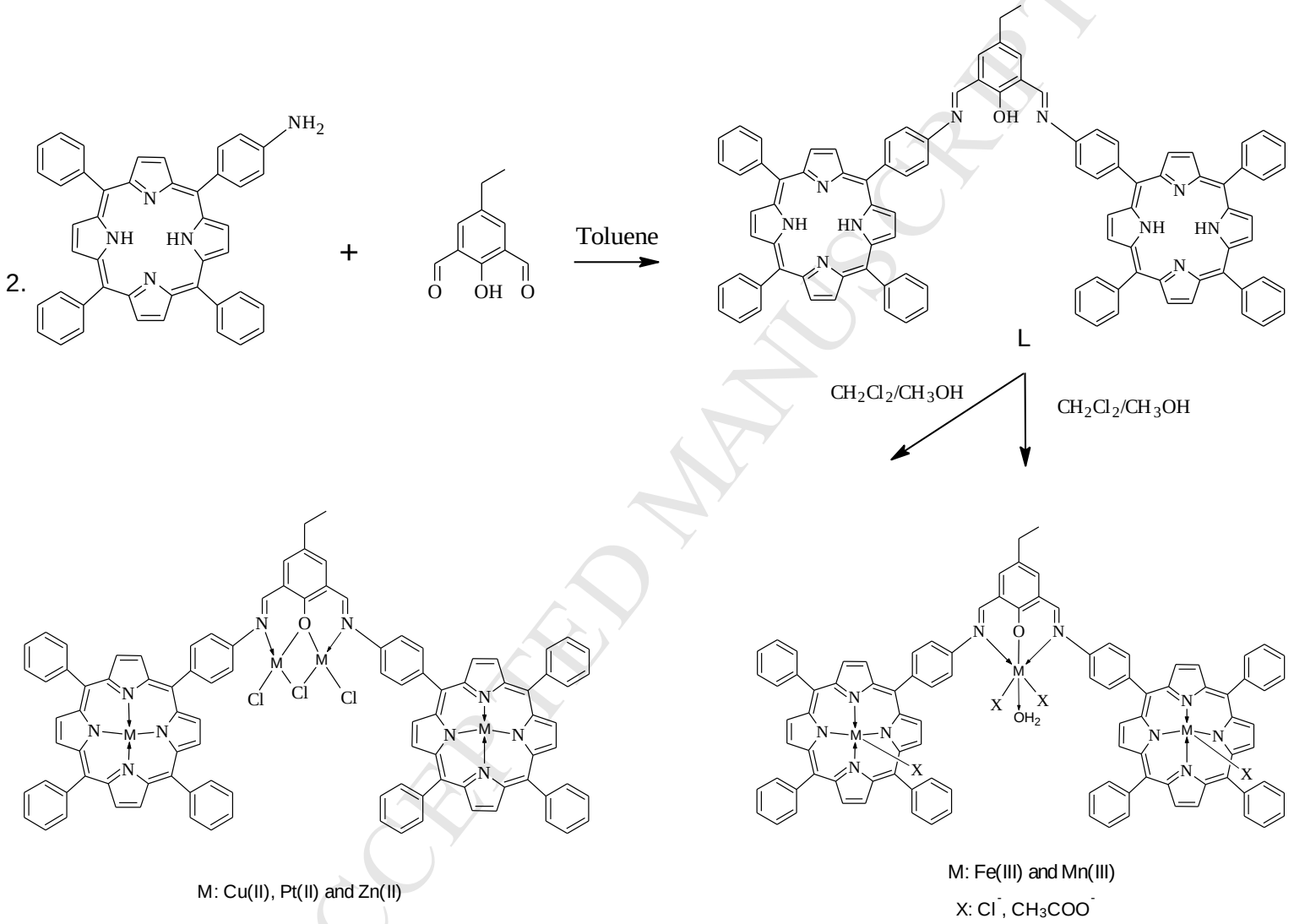

Scheme. Preparation of porphyrin-Schiff base ligand (L) and its metal complexes.

HIGHLIGHTS

- 4-Ethyl-2,6-bis(hydroxymethyl)phenol and 4-ethyl-2,6-diformylphenol compounds have been synthesized and the compounds were, First time, characterized by X-ray single crystallography.

- A new porphyrin Schiff base ligand and its transition metal complexes have been synthesized.

- First time, superoxide dismutase activity and DNA-binding properties of this type compounds were investigated.